RESTRICTED
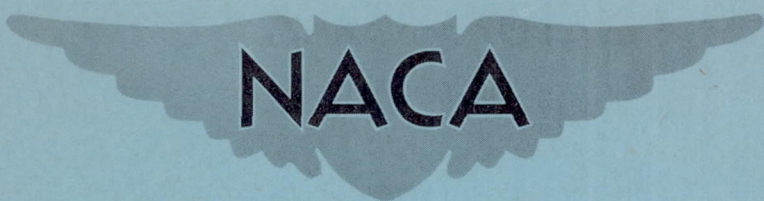
Copy No.
RM No. L9B11

202

NACA RM No. L9B11

NACA

RESEARCH MEMORANDUM

EFFECTS OF HIGH-LIFT AND STALL-CONTROL DEVICES, FUSELAGE,

AND HORIZONTAL TAIL ON A WING SWEPT BACK 42° AT THE

LEADING EDGE AND HAVING SYMMETRICAL

CIRCULAR-ARC AIRFOIL SECTIONS AT

A REYNOLDS NUMBER

OF 6.9×10^6

By

Robert L. Woods and Stanley H. Spooner

Langley Aeronautical Laboratory
Langley Air Force Base, Va.

CLASSIFIED DOCUMENT

This document contains classified information affecting the National Defense of the United States within the meaning of the Espionage Act, USC 50:31 and 32. Its transmission or the revelation of its contents in any manner to an unauthorized person is prohibited by law. Information so classified may be imparted only to persons in the military and naval services of the United States, appropriate civilian officers and employees of the Federal Government who have a legitimate interest therein, and to United States citizens of known loyalty and discretion who of necessity must be informed thereof.

NATIONAL ADVISORY COMMITTEE
FOR AERONAUTICS

WASHINGTON

April 20, 1949

RESTRICTED

NATIONAL ADVISORY COMMITTEE FOR AERONAUTICS

RESEARCH MEMORANDUM

EFFECTS OF HIGH-LIFT AND STALL-CONTROL DEVICES, FUSELAGE,

AND HORIZONTAL TAIL ON A WING SWEPT BACK 42° AT THE

LEADING EDGE AND HAVING SYMMETRICAL

CIRCULAR-ARC AIRFOIL SECTIONS AT

A REYNOLDS NUMBER

OF 6.9×10^6

By Robert L. Woods and Stanley H. Spooner

SUMMARY

The low-speed characteristics of a wing swept back 42° at the leading edge and having various high-lift and stall-control devices and fuselage and horizontal tail vertical positions have been investigated. The wing had an aspect ratio of 3.94, a taper ratio of 0.625, and symmetrical circular-arc airfoil sections. The high-lift and stall-control devices included drooped-nose flaps, extensible round-nose leading-edge flaps, trailing-edge split flaps, and upper-surface fences. The tests were made at a Reynolds number of 6.9×10^6 and a Mach number of 0.15.

The maximum lift of the wing was not critically dependent upon either the span or deflection of the drooped-nose flaps within the flap span range of 0.60 to 0.75 semispan and the deflection range of 20° to 40°. The pitching-moment characteristics, however, varied with change in span or deflection. The maximum lift and pitching-moment characteristics with the extensible leading-edge flaps varied considerably with a change in flap span from 0.55 to 0.70 semispan. For the configurations with drooped-nose flaps or extensible leading-edge flaps, the addition of split flaps resulted in increments in maximum lift coefficient up to 0.19 and 0.34, respectively. The use of the leading-edge devices in conjunction with half-span split flaps resulted in considerable increases in the maximum lift coefficient, but the extensible leading-edge flaps produced more desirable pitching-moment characteristics than did the drooped-nose flaps. Stall-control fences generally had a stabilizing influence on the pitching-moment characteristics in the moderate to high lift range. The addition of a fuselage in the high-wing or midwing positions provided increases in the maximum lift coefficient up to 0.2 for most configurations but was often detrimental to the pitching-moment characteristics.

The configuration with 0.55 semispan extensible leading-edge flaps, split flaps, and high-wing position provided a maximum lift coefficient of 1.52 and stable pitching-moment characteristics. These results are comparable to the lift and moment characteristics obtained for a wing with similar plan form and configuration but incorporating NACA 64_1-112 airfoil sections.

The static longitudinal stability provided by the horizontal tail was the greatest for high tail positions at low angles of attack and for low tail positions at high angles of attack.

INTRODUCTION

The use of sweptback wings incorporating airfoil sections with sharp leading edges has resulted in a need for high-lift and stall-control devices in order to improve the take-off and landing characteristics. Several combinations of leading-edge and trailing-edge high-lift devices have been proposed and some have appeared promising on the basis of data reported in references 1 and 2. A more extensive investigation to evaluate the effectiveness of drooped-nose flaps and extensible leading-edge flaps on a wing swept back 42° at the leading edge and having thin symmetrical circular-arc airfoil sections has been made in the Langley 19-foot pressure tunnel. Also included are data showing effects of wing-fuselage interference which were shown in references 2 and 3 to be of great importance for wings with leading-edge devices, and an investigation to determine the effect of the vertical location of a horizontal tail on the aerodynamic characteristics of the complete model. In addition to the leading-edge devices, the effects of trailing-edge split flaps and stall-control fences were also investigated. The wing had an aspect ratio of 3.94 and a taper ratio of 0.625.

COEFFICIENTS AND SYMBOLS

The data are referred to a set of axes coinciding with the wind axes and originating in the plane of symmetry at the quarter-chord point of the mean aerodynamic chord. All wing coefficients are based upon the dimensions of the basic wing.

C_L lift coefficient $\left(\dfrac{\text{Lift}}{qS}\right)$

$C_{L_{max}}$ maximum lift coefficient

C_D drag coefficient $\left(\dfrac{\text{Drag}}{qS}\right)$

C_m pitching-moment coefficient $\left(\dfrac{\text{Pitching moment}}{qS\bar{c}}\right)$

q free-stream dynamic pressure, pounds per square foot

S wing area, square feet

$\bar{c}$ wing mean aerodynamic chord measured parallel to the plane

of symmetry, 2.942 feet $\left(\dfrac{2}{S}\displaystyle\int_{0}^{b/2} c^2 dy\right)$

c local chord measured parallel to the plane of symmetry

$b/2$ semispan of wing, normal to the plane of symmetry

y spanwise coordinate, normal to plane of symmetry

α angle of attack of wing chord line, degrees

δ_n deflection of drooped-nose flap, degrees

$\dfrac{dC_m}{dC_L}$ rate of change of pitching-moment coefficient with lift
              coefficient

ϵ effective downwash angle, degrees

i_t incidence of horizontal tail with respect to wing chord,
              degrees

q_t/q ratio of effective dynamic pressure at the tail to free-
              stream dynamic pressure

$\dfrac{d\epsilon}{d\alpha}$ rate of change of effective downwash angle with angle of attack

$\dfrac{dC_m}{di_t}$ rate of change of pitching-moment coefficient with tail
              incidence

MODEL

The principle dimensions of the model are shown in figures 1 and 2. Photographs of the model mounted for testing in the Langley 19-foot pressure tunnel are shown as figure 3. The wing, which was of solid steel construction, had symmetrical circular-arc airfoil sections, an aspect ratio of 3.94, and a ratio of tip chord to root chord of 0.625. A straight line connecting the leading edge of the root and theoretical tip chords was swept back 42.05°.

The airfoil sections, taken normal to the line of maximum thickness, had a maximum thickness of 10 percent of the chord at the root and 6.4 percent of the chord at the tip. Parallel to the plane of symmetry the maximum thickness was 7.9 percent of the chord at the root and 5.2 percent of the chord at the tip.

The drooped-nose flaps were hinged on the lower surface and had a chord of approximately 18.4 percent of the wing chord measured parallel to the plane of symmetry. Two spans were tested: one covering the outboard 60 percent of the wing semispan, and the other, the outboard 75 percent. They were constructed so as to provide deflections of 0°, 20°, 30°, and 40°.

The round nose, extensible leading-edge flaps were of constant chord and deflection and were tested with spans of 55 percent and 70 percent of the wing semispan. These flaps extended from the $0.975\frac{b}{2}$ station to the $0.425\frac{b}{2}$ and $0.275\frac{b}{2}$ stations, respectively, as shown in figure 2. A nose radius was obtained by welding a $\frac{1}{2}$-inch steel tube to the steel flaps and then fairing to give a smooth contour.

The trailing-edge split flaps used were of 20 percent chord and covered the inboard 50 percent semispan. They were deflected 60° from the lower surface of the wing in a plane normal to the flap hinge line. For all wing-fuselage tests, the inboard portion of each flap, covering 12.4 percent of the wing semispan, was removed.

The stall-control fences, mounted parallel to the plane of symmetry and with a constant height of 60 percent of the maximum thickness of the root chord (fig. 2) were installed on the wing upper surface for some of the tests. They extended from the wing leading edge to the trailing edge for all configurations except those involving the drooped-nose flaps, in which case they extended from the flap hinge line to the wing trailing edge. In tests with the $0.70\frac{b}{2}$ leading-edge flaps and the $0.75\frac{b}{2}$ drooped-nose flaps, the fences were mounted at a distance of 30 percent of the wing semispan outboard from the plane of symmetry. For all other tests in which fences were used, they were mounted 45 percent of the wing semispan outboard of the plane of symmetry.

The fuselage was of circular cross section with a maximum diameter of 40 percent of the root chord and had a fineness ratio of 10.2. The section of the fuselage intersected by the wing was of constant diameter and had removable blocks to permit attachment to the wing at three vertical positions. The fuselage was constructed of laminated mahogany, lacquered, and sanded smooth.

The horizontal tail had the same plan form as the wing and an area of 0.16 that of the wing. The airfoil sections of the tail, parallel to the plane of symmetry, were NACA 0012-64 sections. The tail length, measured between the quarter-chord points of the wing and tail mean aerodynamic chords and parallel to the plane of symmetry, was approximately twice the wing mean aerodynamic chord. The four vertical positions of the horizontal tail are shown in figure 1 and are given in percent of wing semispan above the wing chord plane extended. The tail incidence was measured with respect to the wing chord plane and was varied by rotating the tail about a line normal to the plane of symmetry and through the quarter-chord point of its mean aerodynamic chord.

TESTS

The tests were conducted in the Langley 19-foot pressure tunnel with the air compressed to approximately 33 pounds per square inch absolute. All tests were made at a Reynolds number of 6.9×10^6, based on the wing mean aerodynamic chord, and a Mach number of 0.15. The lift, drag, and pitching moment were measured by a simultaneously recording balance system through an angle-of-attack range from near zero lift to beyond maximum lift. Stall characteristics were studied by observation of the behavior of wool tufts attached to the upper surface of the wing.

REDUCTION OF DATA

All data have been reduced to standard nondimensional coefficients and have been corrected for support tare and interference effects and for air-stream misalinement. The jet-boundary corrections to the angle of attack and drag coefficient were calculated from reference 4 and were as follows:

$$\Delta\alpha = 1.00C_L$$

$$\Delta C_D = 0.0152C_L{}^2$$

The correction to the pitching-moment coefficient for configurations without a horizontal tail was

$$\Delta C_m = 0.0041C_L$$

and for configurations with a horizontal tail was

$$\Delta C_m = 0.0102C_L$$

All corrections were added to the data.

The downwash angles were computed from the pitching-moment coefficients of the model with and without the horizontal tail. The dynamic-pressure ratio q_t/q was determined from the ratio of tail effectiveness $\frac{dC_m}{di_t}$ at a given angle of attack to the effectiveness at zero lift.

RESULTS AND DISCUSSION

The lift, drag, and pitching-moment characteristics of the wing equipped with various high-lift and stall-control devices are presented in figures 4 to 10. The characteristics of the various wing-fuselage combinations are presented in figures 11 to 14. A summary of some of the important characteristics of the wing for various configurations is given in tables I and II. The stall progressions are shown in figures 15 to 17. To assist in interpreting the lift-drag variations in terms of power-off gliding characteristics, contours of constant gliding speed and constant vertical (sinking) speed are superimposed on the lift-drag polars of several configurations and are presented in figure 18. The longitudinal stability characteristics of the model equipped with the horizontal tail are shown in figures 19 to 23.

Although some of the data presented herein have been reported in reference 2, they are included for the sake of completeness.

Characteristics of Basic Wing

The plain wing and the wing with the split flaps exhibited poor lift, drag, and pitching-moment characteristics. Both configurations were found to have nonlinear variations of lift and pitching moment with angle of attack and rapid increases in drag at moderate lift coefficients (fig. 4). The values of maximum lift coefficient were approximately 0.84 and 0.95 for the plain wing and for the wing with the split flaps, respectively. The pitching-moment curve for both configurations became sharply positive as the stall began on the outer portions of the wing and then broke in a negative direction as the stall progressed inward toward the root section (fig. 15(a)).

The effect of upper-surface stall-control fences was quite pronounced. By delaying the onset of the tip stall, the fences extended the lift curve in a manner such as to increase $C_{L_{max}}$ slightly and to considerably reduce the angle of attack for $C_{L_{max}}$ (fig. 4). The positive breaks in the pitching-moment curves were delayed until $C_{L_{max}}$ was reached (fig. 4). A more complete investigation of stall-control fences reported in reference 1 showed that equally good results could be obtained with a much smaller fence, provided it was located at the wing leading edge.

Leading-Edge Flap Investigation

Drooped-nose flaps.- A considerable increase in $C_{L_{max}}$ of the basic
wing was obtained by the deflection of the drooped-nose flaps, although
large variations in $\dfrac{dC_m}{dC_L}$ were evident throughout the lift range. With
the $0.60\dfrac{b}{2}$ drooped-nose flaps and the split flaps, maximum lift coefficients
of 1.26, 1.28, and 1.29 were obtained with drooped-nose flap deflections
of 20°, 30°, and 40°, respectively (fig. 5). Thus, the amount of deflection
within this range appeared to have little effect on the maximum lift. In
the case of the $0.75\dfrac{b}{2}$ drooped-nose-flap configuration (fig. 6) $C_{L_{max}}$ was
substantially the same as that for the $0.60\dfrac{b}{2}$ configuration at deflections
of 30° and 40° and slightly less at a deflection of 20°. In a previous
investigation (reference 5) of a 45° sweptback wing with similar airfoil
sections, however, it was found that the values of $C_{L_{max}}$ decreased
rapidly as the span of the drooped-nose flap was reduced below $0.50\dfrac{b}{2}$.
As can be seen in figures 4 to 7, the increment in $C_{L_{max}}$ due to the
split flaps (about 0.10) was the same with the $0.60\dfrac{b}{2}$ drooped-nose flaps
as with the plain wing, whereas with the $0.75\dfrac{b}{2}$ drooped-nose flaps the
increment was somewhat larger (0.17). Above a lift coefficient of
about 0.5, the drag coefficients of the wing with the $0.75\dfrac{b}{2}$ drooped-nose
flaps were appreciably smaller than those of the wing with the $0.60\dfrac{b}{2}$
drooped-nose flaps for configurations both with and without split flaps.

The pitching-moment characteristics of the configurations employing
the drooped-nose flaps were generally unfavorable, with large variations
in $\dfrac{dC_m}{dC_L}$ occurring throughout the lift range. The typical stall
progressions presented in figure 15 explain these large variations,
particularly at the angles of attack at which air flow separation occurs.
For the configuration of split flaps and $0.60\dfrac{b}{2}$ drooped-nose flaps
deflected 30° (fig. 5), a stable break in the pitching-moment curve
occurred above a lift coefficient of about $0.75C_{L_{max}}$. The stall
progressions show that the stalled area began just behind the inboard
end of the drooped-nose flaps and progressed inward more rapidly than
it progressed outward, thus causing a large negative slope in the
moment curve. At $C_{L_{max}}$ the stalled area expanded rapidly inboard
to envelope the entire root section and cause the pitching-moment curve
to break in a negative direction. For the configurations with
the $0.75\dfrac{b}{2}$ drooped-nose flaps, both with and without split flaps, a large
unstable pitching-moment break at $C_{L_{max}}$ was obtained for all flap
deflections investigated.

These results indicate that for a 42° sweptback wing the $0.75\frac{b}{2}$ drooped-nose flaps appear to offer some increases in L/D ratios in the higher lift range but no advantages over the $0.60\frac{b}{2}$ flaps in the maximum lift attainable and are inferior from stability considerations.

The main function of the upper-surface fences was to reduce the large variations in $\frac{dC_m}{dC_L}$ in the range up to $C_{L_{max}}$ by alleviating the spanwise flow towards the tips which contributed to early tip stalling (fig. 8).

Extensible leading-edge flaps.- The value of $C_{L_{max}}$ obtained for the wing equipped with the $0.70\frac{b}{2}$ extensible leading-edge flaps but without the split flaps was reported in reference 2 to be 1.18, which was somewhat greater than that shown herein for the $0.75\frac{b}{2}$ drooped-nose flaps. The addition of the split flaps to the wing with the $0.70\frac{b}{2}$ extensible leading-edge flaps, however, resulted in a $C_{L_{max}}$ of 1.52 (fig. 9), an increment of 0.34 as compared with an increment of only 0.17 obtained by adding the split flaps to the wing with the $0.75\frac{b}{2}$ drooped-nose flaps. The maximum lift coefficient obtained using the $0.55\frac{b}{2}$ extensible leading-edge flaps in conjunction with the split flaps was 1.35, which is slightly greater than that obtained with the $0.60\frac{b}{2}$ drooped-nose flaps. These values are comparable to those obtained in a previous investigation of a wing with similar plan form and leading-edge flap configuration but incorporating NACA 64_1-112 airfoil sections (reference 3).

The pitching-moment characteristics in the range up to the stall were generally more favorable than those of the drooped-nose-flap configurations. With the $0.70\frac{b}{2}$ extensible leading-edge flaps and split flaps, the pitching-moment curve broke in a slightly positive direction at maximum lift, whereas with the $0.55\frac{b}{2}$ extensible leading-edge flaps and split flaps $\frac{dC_m}{dC_L}$ became negative considerably below $C_{L_{max}}$ and at $C_{L_{max}}$ large negative moments were obtained. For this 42° sweptback wing, a span of about $0.65\frac{b}{2}$ for the extensible leading-edge flaps probably would supply favorable pitching-moment characteristics without a large sacrifice in $C_{L_{max}}$.

The effect of the stall-control fences was similar to that on the drooped-nose-flap configuration. The fences provided more stable moment characteristics in the moderate to high-lift range, although for the wing with the short-span extensible leading-edge flap this effect was small. For the $0.70\frac{b}{2}$ extensible flap configuration, however, the slightly positive break of the moment curve at $C_{L_{max}}$ was reversed and became slightly negative.

The glide characteristics of the model with several flap configurations and with an assumed wing loading of 40 pounds per square foot are shown in figure 18. No attempt has been made to account for the changes in lift due to trimming of the pitching moments nor for the effects of a fuselage, landing gear, nacelles, or other protuberances. Inasmuch as this presentation represents a steady state glide, the relative perform-ance of a landing maneuver, which usually involves accelerations, is not specifically indicated. However, the general effects of the flaps in a steady glide are readily shown. The configuration of $0.70\frac{b}{2}$ exten-sible leading-edge flaps and split flaps provided a minimum sinking speed of 30 feet per second which was the lowest obtained with the flapped configurations investigated. At this sinking speed, a gliding speed of approximately 120 miles per hour was obtained. The sinking speed of 30 feet per second is higher than the presently established limit of 25 feet per second reported in reference 6, although this could probably be reduced somewhat by decreasing the split-flap deflection. The $0.55\frac{b}{2}$ extensible leading-edge flaps and the $0.60\frac{b}{2}$ drooped-nose flaps showed about the same glide characteristics but both had higher horizontal and vertical speeds than the $0.70\frac{b}{2}$ exten-sible flap configuration.

Wing Fuselage Investigation

The wing, equipped with various high-lift and stall-control devices, was tested in conjunction with a fuselage mounted in high-wing, midwing, and low-wing positions, and the results summarized in table I(b).

The addition of a fuselage in any of the three vertical positions to the plain wing or wing with split flaps caused no large changes in the wing characteristics (reference 2). A slight increase in $C_{L_{max}}$ with the high-wing and midwing arrangements and a moderate destabilizing effect throughout the lift range were obtained.

For the wing with leading-edge devices, the effects of a fuselage were more pronounced. In the case of the wing with $0.60\frac{b}{2}$ drooped-nose flaps deflected 30°, split flaps, and upper-surface fences (fig. 11),

the addition of a fuselage in the high-wing or midwing position caused an increase in $C_{L_{max}}$ of 0.10 even though the inboard 25 percent of the split flaps were removed to allow for installation of the fuselage. In addition, above a lift coefficient of 1.0 the drag coefficients were reduced considerably with these high-wing and midwing configurations. The values of $C_{L_{max}}$ and C_D obtained with the low-wing position were about the same as those obtained without the fuselage but with the split flaps extending into the plane of symmetry. The higher values of $C_{L_{max}}$ obtained with the high-wing and midwing positions probably resulted from the action of the fuselage in delaying the root stall to a higher angle of attack. The pitching moments of these configurations, however, became unstable near $C_{L_{max}}$ in contrast to the stable moments obtained with the low-wing and fuselage-off conditions. Reference to the stall studies of figure 16 indicates that in the high-wing and midwing positions, the fuselage prevented the stall from enveloping the root sections until after the tips had stalled, thus producing the unstable pitching-moment characteristics. With the low-wing configuration, however, some root stalling occurred and a small stable pitching moment at $C_{L_{max}}$ resulted.

The effects of the fuselage on the lift and pitching-moment characteristics of the wing with $0.60\frac{b}{2}$ drooped-nose flaps with split flaps off were about the same as the effects with split flaps on. In the low-wing position, however, an unstable pitching moment at $C_{L_{max}}$ was obtained for the configuration with split flaps off although this was preceded by a large stable variation near $C_{L_{max}}$ (fig. 12).

The effects on the lift and drag coefficients of adding a fuselage to the wing with $0.55\frac{b}{2}$ extensible leading-edge flaps and split flaps were similar to those for the $0.60\frac{b}{2}$ drooped-nose-flap configuration, except that in the high-wing position the increment in $C_{L_{max}}$ was considerably larger and resulted in a maximum lift coefficient of 1.52 (fig. 13). The pitching-moment variations at $C_{L_{max}}$ for the high-wing and midwing positions, however, were stable in contrast to the unstable variations obtained with the drooped-nose flap. This effect is explained by a study of the stall progressions of figure 17, which shows that the outboard wing sections for these configurations remained unstalled throughout the lift range. For the low-wing position, a large stable pitching-moment variation was obtained at a lift coefficient just under that of $C_{L_{max}}$. The lift continued to increase to a second maximum at a very high angle of attack, however, and at this point a large unstable pitching-moment variation occurred. Reference to figure 17 shows that this instability is associated with the onset of tip stalling.

For the configuration with the $0.70\frac{b}{2}$ extensible leading-edge flaps and split flaps, the addition of the fuselage in either the high-wing or midwing positions did not appreciably alter the value of $C_{L_{max}}$ but did result in a small decrease in drag coefficient (fig. 14). With the low-wing position, the value of $C_{L_{max}}$ was actually reduced about 0.10 from that obtained with the fuselage off. However, in reference 2 and in unpublished data it was shown that for this same configuration, but with split flaps off, the value of $C_{L_{max}}$ was increased by increments of 0.15 to 0.20 by the addition of a fuselage in any of the three vertical positions. The final break in the pitching-moment curves was in an unstable direction for all wing positions, although for the low-wing position there was a sharp stable break immediately preceding $C_{L_{max}}$.

The effect of upper-surface fences was found to be about the same as that for configurations without the fuselage, and the data have therefore not been included in this paper.

In general, the effects of a fuselage on the various wing configurations tested were found to be similar to those obtained in previous tests of an NACA 64_1-112 wing of similar plan form (reference 3).

Horizontal Tail Investigation

A summary of the longitudinal stability characteristics of the low-wing-fuselage combination with a sweptback horizontal tail is presented in table II. Also included is the tail effectiveness parameter $\frac{dC_m}{di_t}$ at $C_L = 0$ which was used as a basis in determining q_t/q. In figures 19 to 22, data are presented showing the lift and pitching-moment characteristics of the combination with the tail located in several vertical positions and with various leading-edge devices on the wing. In figure 23 is shown the variation of neutral-point location with lift coefficient for the various configurations tested.

It can be seen that in the low to moderate lift range the greatest degree of stability was obtained with the horizontal tail in the high positions. This effect is the result of the relatively low values of $\frac{d\epsilon}{d\alpha}$, dynamic pressures at the tail equal to free-stream dynamic pressures, and (as shown in table II) relatively high values of $\frac{dC_m}{di_t}$ which indicate little fuselage interference. Conversely, in the range near $C_{L_{max}}$ the stability was the greatest for the lowest tail position. With the exception of the lowest tail position investigated, the contribution of the tail to the stability in the stalling range was small.

The dynamic-pressure ratios shown in figures 19 to 22 indicate that the tail in the low position was first enveloped by the wing wake at low angles of attack and then at angles of attack near those for $C_{L_{max}}$ it emerged from the wake which rose with respect to the wing chord plane extended. The angle of attack at which the tail entered the wake became progressively greater as the tail height was increased. The favorable effects on $\frac{d\epsilon}{d\alpha}$ of the wing wake being located above the tail in its lowest position probably explains the large contribution to stability by the tail in this position.

The influence of the wing stall progression on the stability contributed by the tail appeared to be slight. In the high-lift range, the effective values of $\frac{d\epsilon}{d\alpha}$ at the tail for the unflapped wing, where stalling began at the tips, were about the same as for the flapped configurations, where initial stalling occurred near the root.

The addition of the $0.60\frac{b}{2}$ drooped-nose flaps together with the split flaps resulted in a slight rearward shift of the neutral point at low lift coefficients and a slight forward shift at higher lift coefficients (fig. 23). The addition of either the $0.55\frac{b}{2}$ or the $0.70\frac{b}{2}$ extensible leading-edge flaps and split flaps, on the other hand, resulted in a slight forward shift of the neutral point which was probably caused by the increased wing area ahead of the center-of-gravity position under consideration.

In general, the effects of the various tail positions and the high-lift and stall-control devices on the longitudinal stability characteristics of the model were similar to those obtained for a model with a similar plan form but having NACA 64_1-112 airfoil sections (reference 7).

CONCLUSIONS

From the results of tests to determine the effects of high-lift and stall-control devices, a fuselage, and a horizontal tail on a wing sweptback 42° at the leading edge and having symmetrical circular-arc airfoil sections, the following conclusions have been drawn:

1. The maximum lift of the wing was not critically dependent upon either the span or deflection of the drooped-nose flaps within the flap span range of 0.60 to 0.75 semispan and the deflection range of 20° to 40°. The pitching-moment characteristics, however, varied with change in span or deflection. The maximum lift and pitching-moment characteristics with the extensible leading-edge flaps varied considerably with a change in flap span from 0.55 to 0.70 semispan.

2. For the configurations with drooped-nose flaps or extensible
leading-edge flaps, the addition of split flaps resulted in increments
in maximum lift coefficient up to 0.19 and 0.34, respectively.

3. The use of the leading-edge devices in conjunction with half-
span split flaps resulted in considerable increases in the maximum
lift coefficient, but the extensible leading-edge flaps produced more
desirable pitching-moment characteristics than did the drooped-nose flaps.

4. Stall-control fences generally had a stabilizing influence on the
pitching-moment characteristics in the moderate to high-lift range.

5. The addition of a fuselage in the high-wing or midwing positions
provided increases in the maximum lift coefficient up to 0.2 for most
configurations but was often detrimental to the pitching-moment
characteristics.

6. The configuration with 0.55 semispan extensible leading-edge
flaps, split flaps, and high-wing position provided a maximum lift
coefficient of 1.52 and stable pitching-moment characteristics. These
results are comparable to the lift and moment characteristics obtained
for a wing with similar plan form and configuration but incorporating
NACA 64_1-112 airfoil sections.

7. The static longitudinal stability provided by the horizontal
tail was the greatest for high-tail positions at low angles of attack
and for low-tail positions at high angles of attack.

Langley Aeronautical Laboratory
    National Advisory Committee for Aeronautics
        Langley Air Force Base, Va.

REFERENCES

1. Weil, Joseph, Comisarow, Paul, and Goodson, Kenneth W.: Longitudinal
      Stability and Control Characteristics of an Airplane Model Having
      a 42.8° Sweptback Circular-Arc Wing with Aspect Ratio 4.00, Taper
      Ratio 0.50, and Sweptback Tail Surfaces. NACA RM No. L7G28, 1947.

2. Neely, Robert H., and Koven, William: Low-Speed Characteristics in
      Pitch of a 42° Sweptback Wing with Aspect Ratio 3.9 and Circular-
      Arc Airfoil Sections. NACA RM No. L7E23, 1947.

3. Graham, Robert R., and Conner, D. William: Investigation of High-
      Lift and Stall-Control Devices on an NACA 64-Series 42° Sweptback
      Wing with and without Fuselage. NACA RM No. L7G09, 1947.

4. Eisenstadt, Bertram J.: Boundary-Induced Upwash for Yawed and
      Swept-Back Wings in Closed Circular Wind Tunnels. NACA TN
      No. 1265, 1947.

5. Guryansky, Eugene R., and Lipson, Stanley: Effect of High-Lift
      Devices on the Longitudinal and Lateral Characteristics of
      a 45° Sweptback Wing with Symmetrical Circular-Arc Sections.
      NACA RM No. L8D06, 1948.

6. Gustafson, F. B., and O'Sullivan, William J., Jr.: The Effect of
      High Wing Loading on Landing Technique and Distance, with
      Experimental Data for the B-26 Airplane. NACA ARR No. L4K07, 1945.

7. Spooner, Stanley H., and Martina, Albert P.: Longitudinal Stability
      Characteristics of a 42° Sweptback Wing and Tail Combination at
      a Reynolds Number of 6.8×10^6. NACA RM No. L8E12, 1948.

TABLE I

SUMMARY OF THE CHARACTERISTICS OF A CIRCULAR-ARC 42° SWEPTBACK

WING WITH VARIOUS HIGH-LIFT AND STALL-CONTROL DEVICES AND FUSELAGE POSITIONS

(a) Fuselage off.
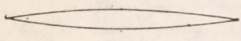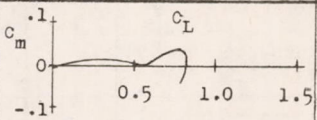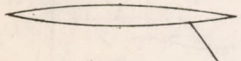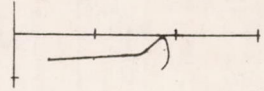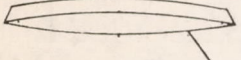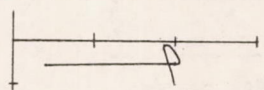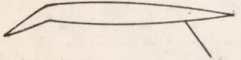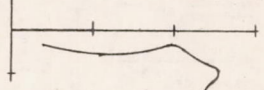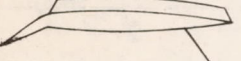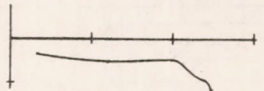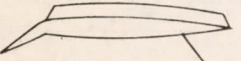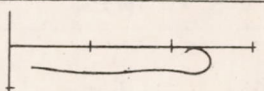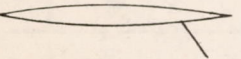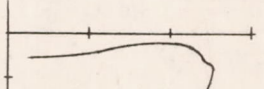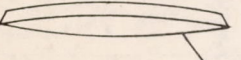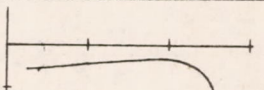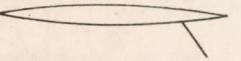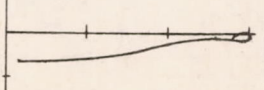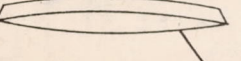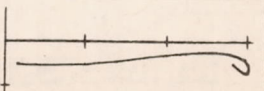
Flap configuration	Upper surface fences	$c_{L_{max}}$	$\alpha_{c_{L_{max}}}$	C_m-curve	Figure
Plain wing	off	0.84	21.0		4
Split	off	0.95	16.0		4
Split	on	1.02	11.5		4
0.60b/2 drooped nose and split. $\delta_n = 30°$.	off	1.28	20.5		8
0.60b/2 drooped nose and split. $\delta_n = 30°$.	on	1.26	19.3		8
0.75b/2 drooped nose and split. $\delta_n = 30°$.	on	1.28	19.4		8
0.55b/2 extensible leading edge and split.	off	1.35	20.4		10
0.55b/2 extensible leading edge and split.	on	1.34	21.4		10
0.70b/2 extensible leading edge and split.	off	1.52	21.2		9
0.70b/2 extensible leading edge and split.	on	1.52	20.6		9

NACA

TABLE I.- Concluded

(b) Wing-fuselage combinations.
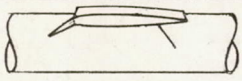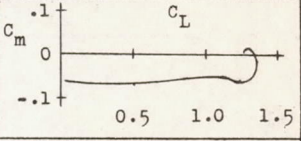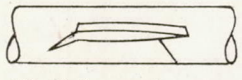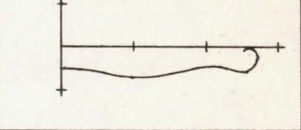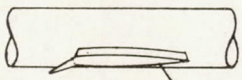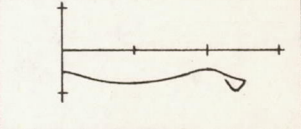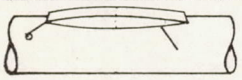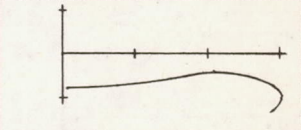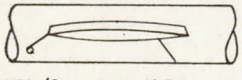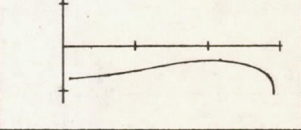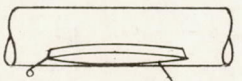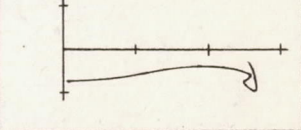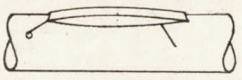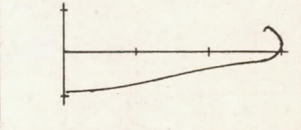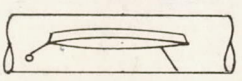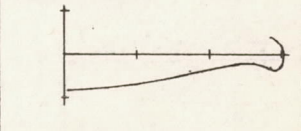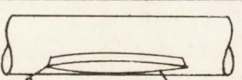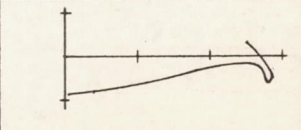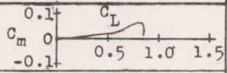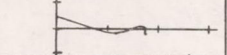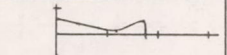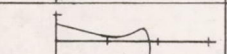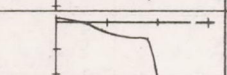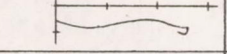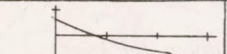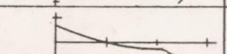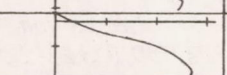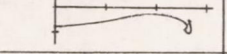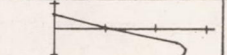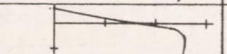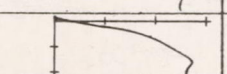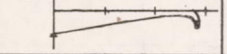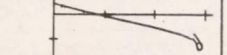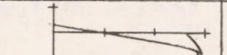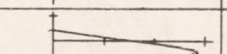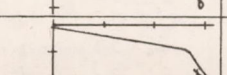
Flap configuration	Upper surface fences	Wing fuselage	$C_{L_{max}}$	$\alpha_{C_{L_{max}}}$	C_m-curve	Figure
0.60b/2 drooped nose and split. $\delta_n = 30°$.	on	high wing	1.35	20.4		11
0.60b/2 drooped nose and split. $\delta_n = 30°$.	on	mid-wing	1.36	21.4		11
0.60b/2 drooped nose and split. $\delta_n = 30°$	on	low wing	1.25	19.0		11
0.55b/2 extensible leading edge and split.	on	high wing	1.52	22.6		13
0.55b/2 extensible leading edge and split.	on	mid-wing	1.44	24.5		13
0.55b/2 extensible leading edge and split.	on	low wing	1.35	26.4		13
0.70b/2 extensible leading edge and split.	on	high wing	1.53	20.2		14
0.70b/2 extensible leading edge and split.	on	mid-wing	1.54	20.6		14
0.70b/2 extensible leading edge and split.	on	low wing	1.42	22.6		14

In the first C_m-curve cell: C_m axis marked .1, 0, -.1; C_L axis marked 0.5, 1.0, 1.5.

NACA

TABLE II

SUMMARY OF LONGITUDINAL STABILITY CHARACTERISTICS OF

42° SWEPTBACK WING-FUSELAGE COMBINATION WITH HORIZONTAL TAIL

Configuration	Tail height (percent b/2 above chord plane extended)	C_m-curve	$d\epsilon/d\alpha$ measured values in low lift range	dC_m/di_t at $C_L=0$
Flaps off low wing	Tail off		– – – –	– – – –
	46.6		0.32	-0.0160
	33.9		0.45	-0.0160
	21.1		0.45	-0.0160
	-1.1		0.45	-0.0153
0.60b/2 drooped nose deflected 30°, split flaps, and fences. Low wing.	Tail off		– – – –	– – – –
	46.6		0.40	-0.0176
	33.9		0.43	-0.0170
	21.1		0.48	-0.0166
	-1.1		0.48	-0.0147
0.55b/2 extensible leading edge flaps, split flaps, and fences. Low wing.	Tail off		– – – –	– – – –
	46.6		0.45	-0.0173
	33.9		0.45	-0.0165
	21.1		0.48	-0.0155
	-1.1		0.45	-0.0146
0.70b/2 extensible leading edge flaps, split flaps, and fences. Low wing.	Tail off		– – – –	– – – –
	46.6		0.36	-0.0170
	33.9		0.48	-0.0168
	21.1		0.48	-0.0160
	-1.1		0.50	-0.0150

Figure 1.— Geometry of wing, fuselage, and horizontal tail.
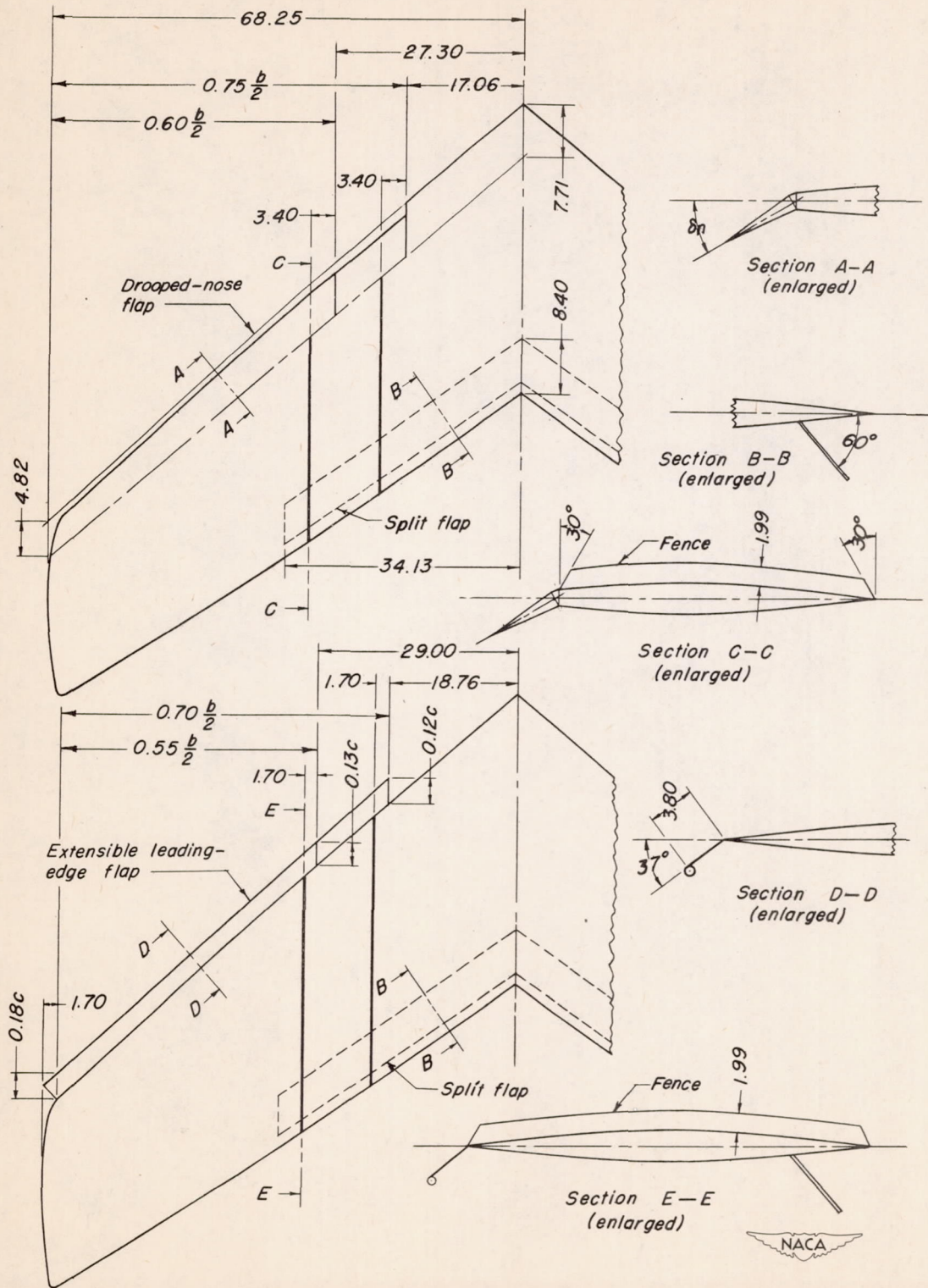
Figure 2.— Details of high-lift and stall-control devices on a
42° sweptback wing.
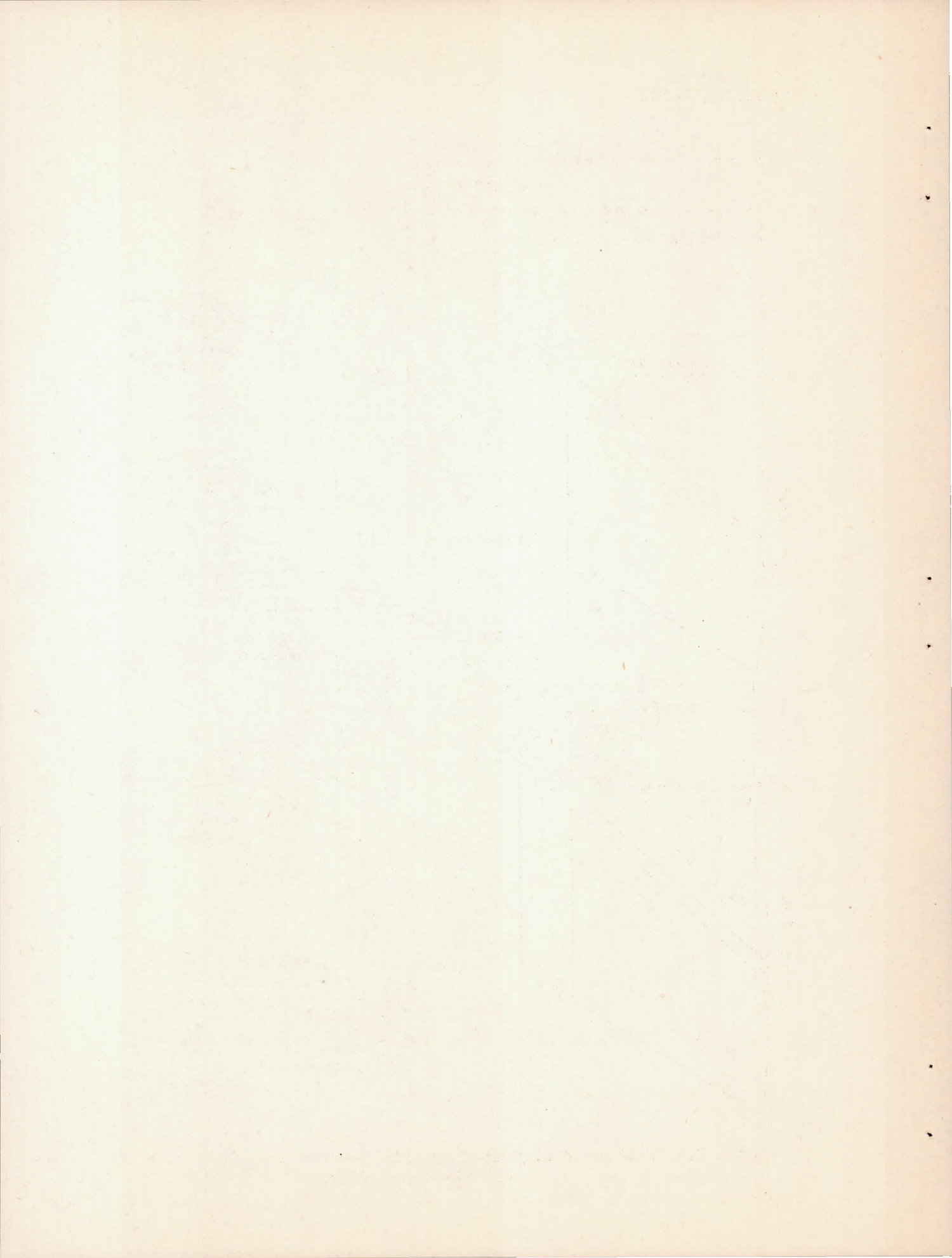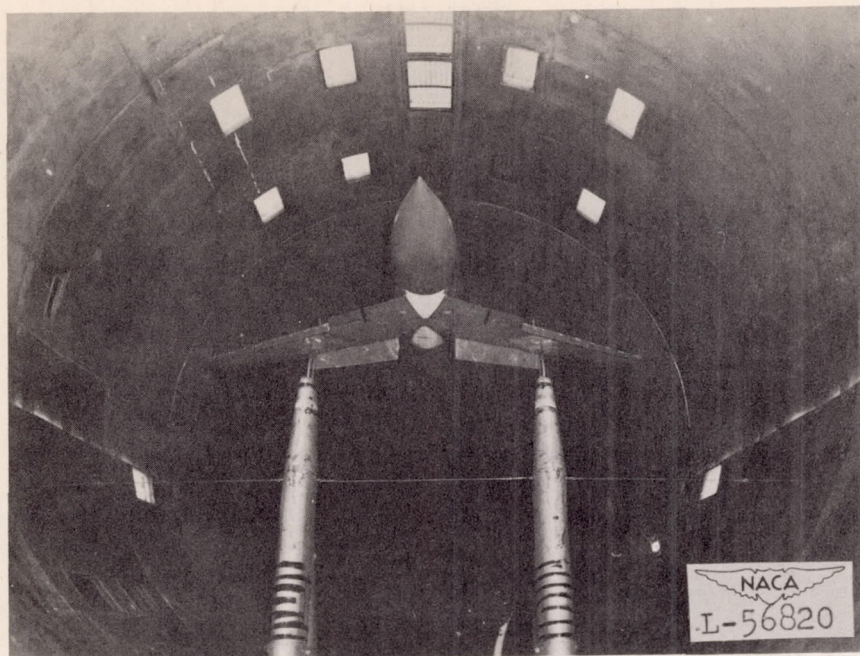
(a) $0.60\frac{b}{2}$ drooped-nose flaps deflected 40°.
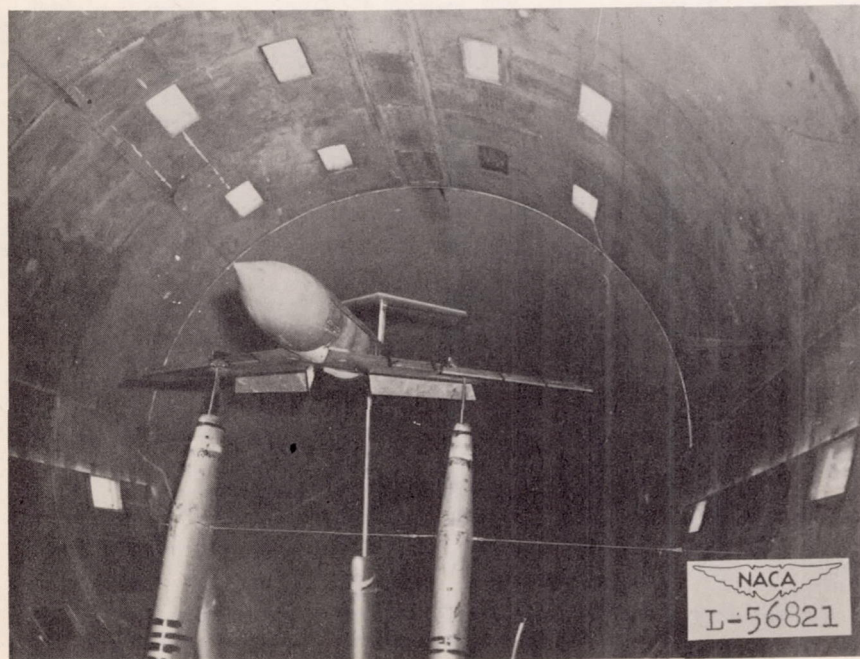
(b) $0.55\frac{b}{2}$ extensible leading-edge flaps.   Horizontal
tail in highest position.

Figure 3.- The 42° sweptback wing-fuselage combination mounted for
testing in the Langley 19-foot pressure tunnel. Split flaps and
upper surface fences on; low-wing position.
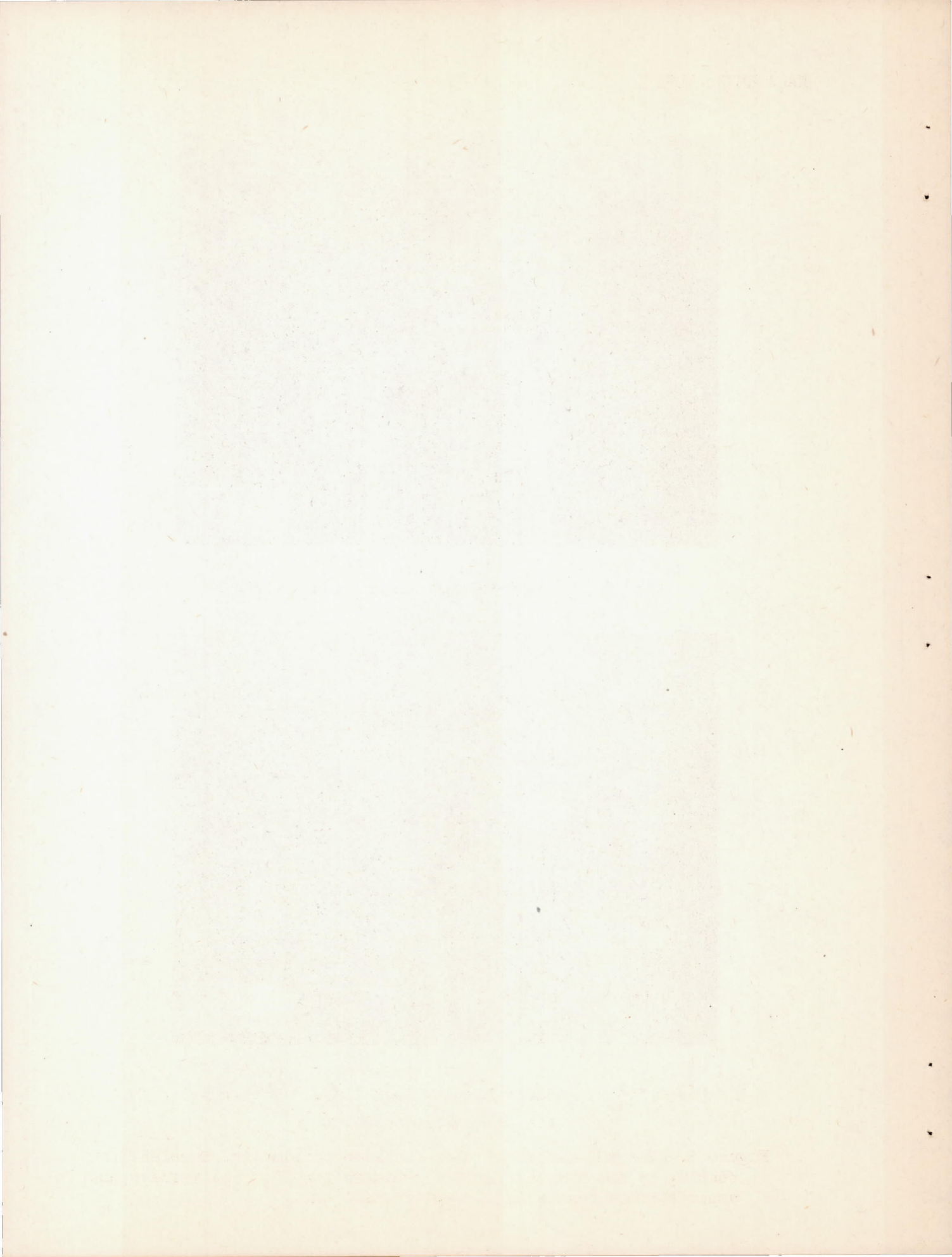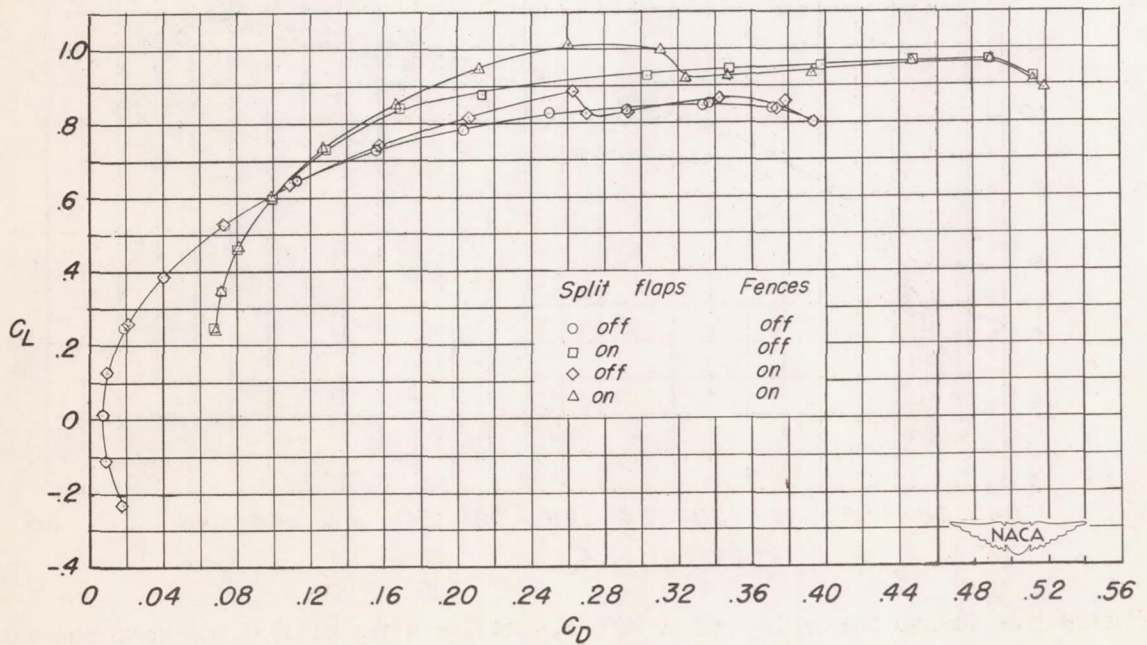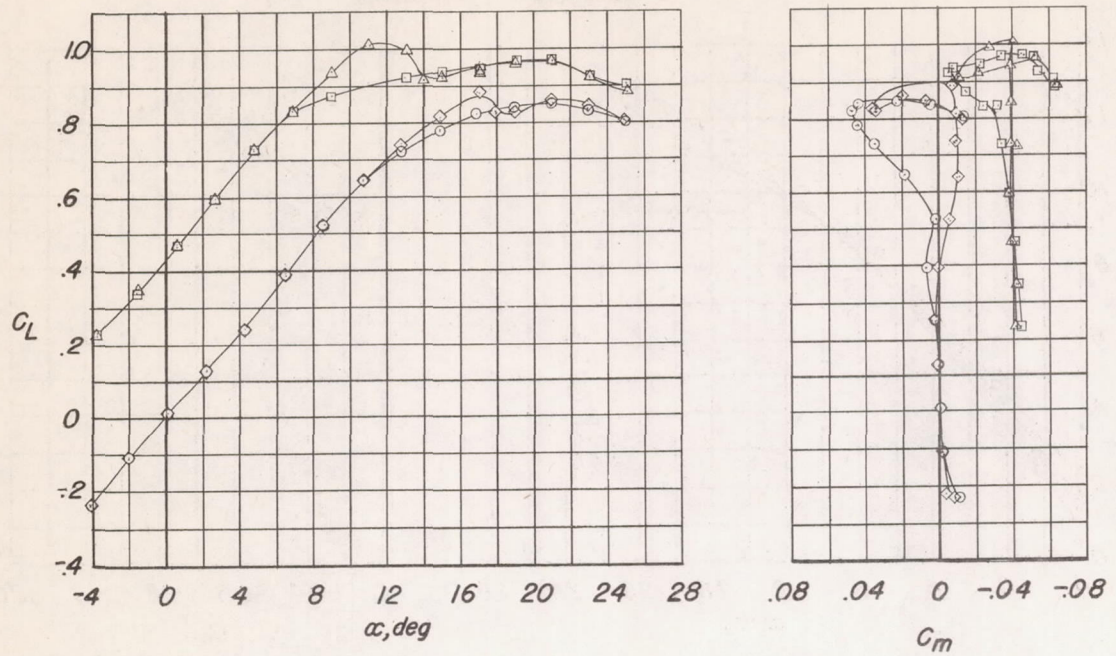
Figure 4.— Characteristics of a 42° sweptback wing with and without split flaps and upper–surface stall—control fences.
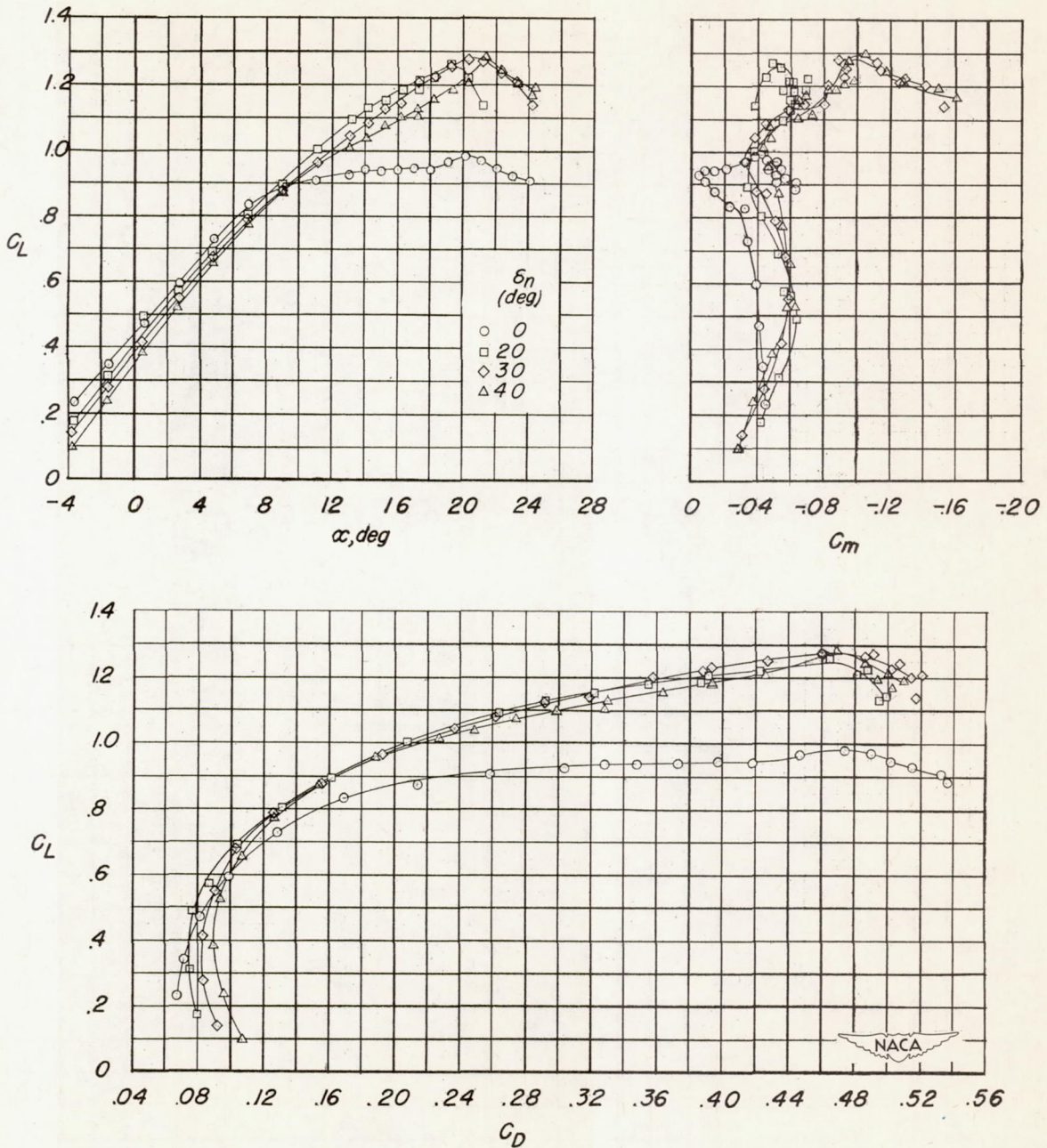
Figure 5.— Characteristics of a 42° sweptback wing with $0.60\frac{b}{2}$ drooped—nose flaps and split flaps.
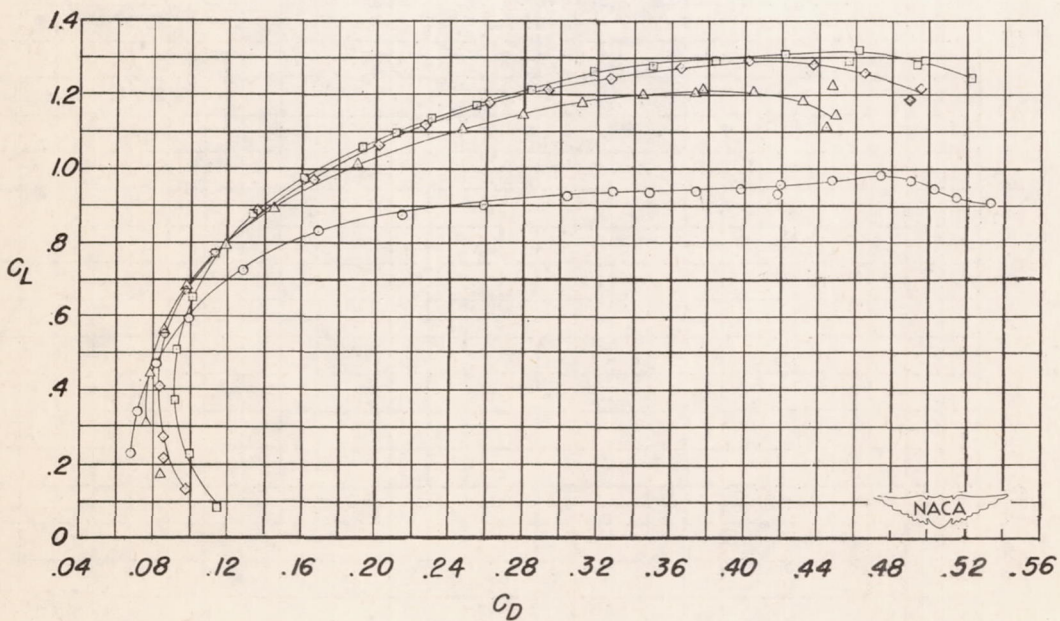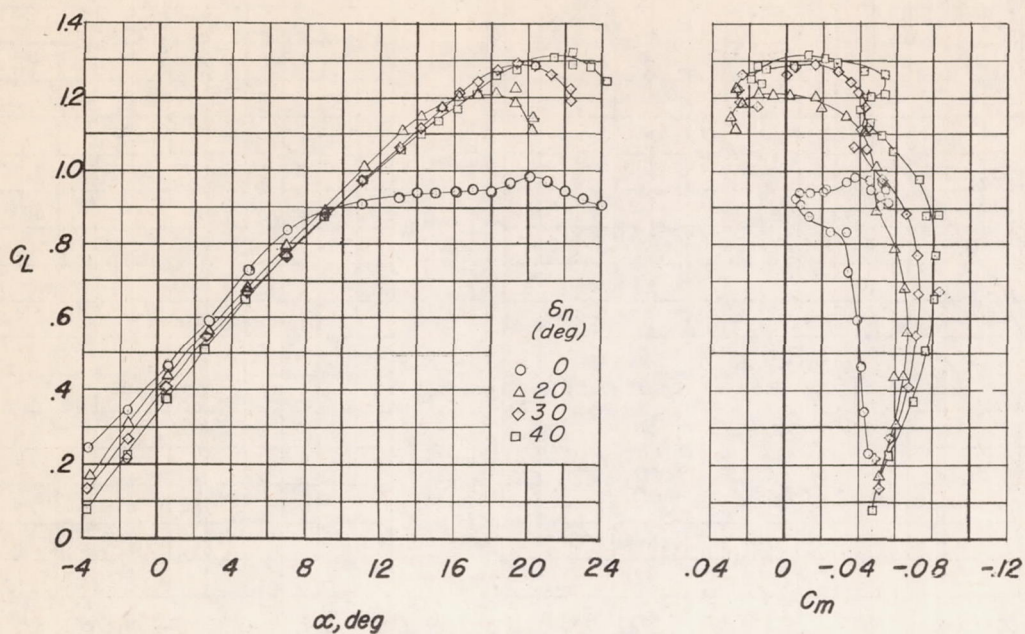
Figure 6.— Characteristics of a $42°$ sweptback wing with $0.75\frac{b}{2}$ drooped-nose flaps and split flaps.

Drooped-nose-
flap span   Split flaps
○   0.60 b/2   on
□   .75 b/2   on
◇   .60 b/2   off
△   .75 b/2   off

C_L

α, deg

C_m

C_L

C_D

NACA
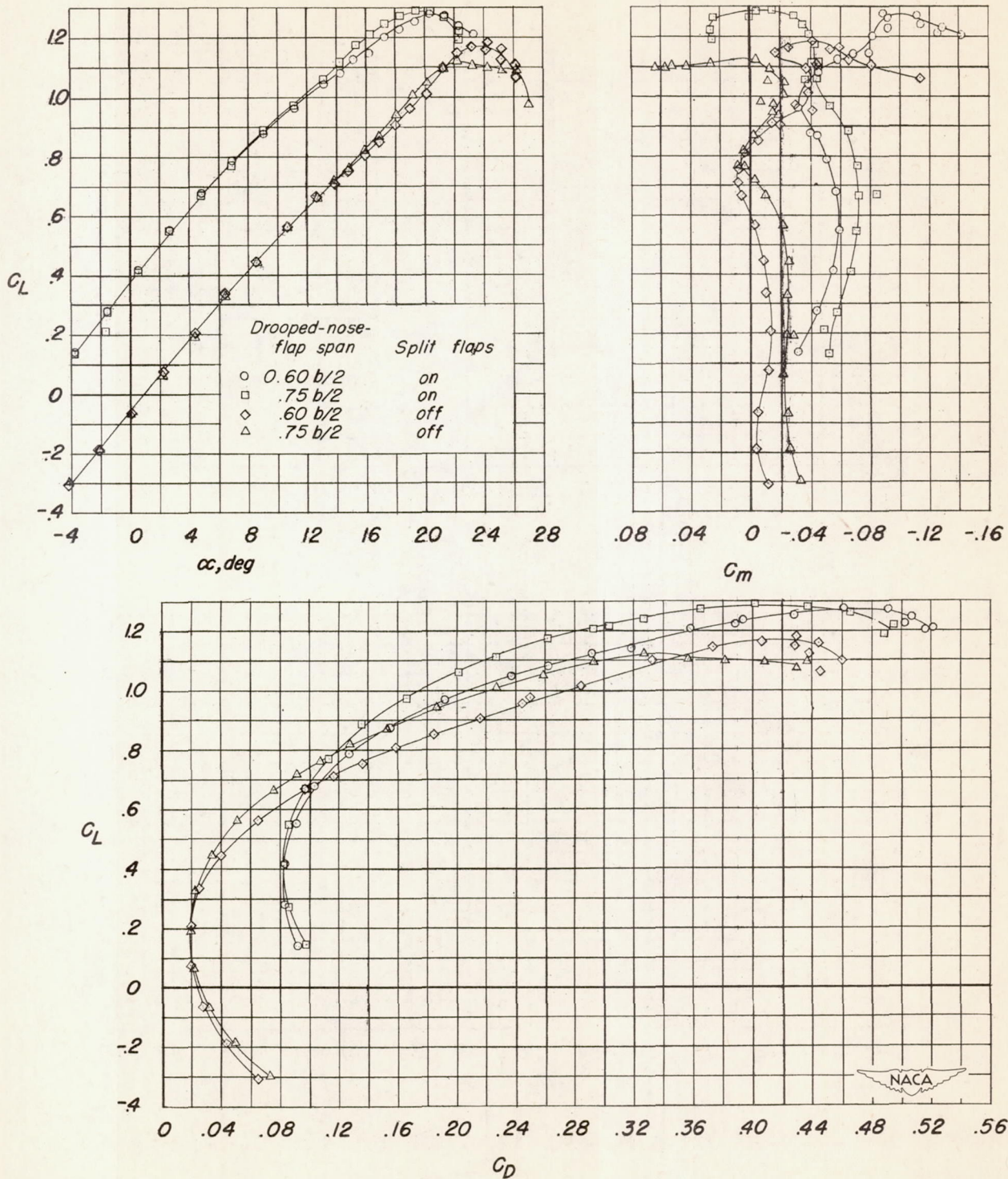
Figure 7.— Characteristics of a 42° sweptback wing with $0.60\frac{b}{2}$
and $0.75\frac{b}{2}$ drooped—nose flaps with and without split flaps.
$\delta_n = 30^{\circ}$.
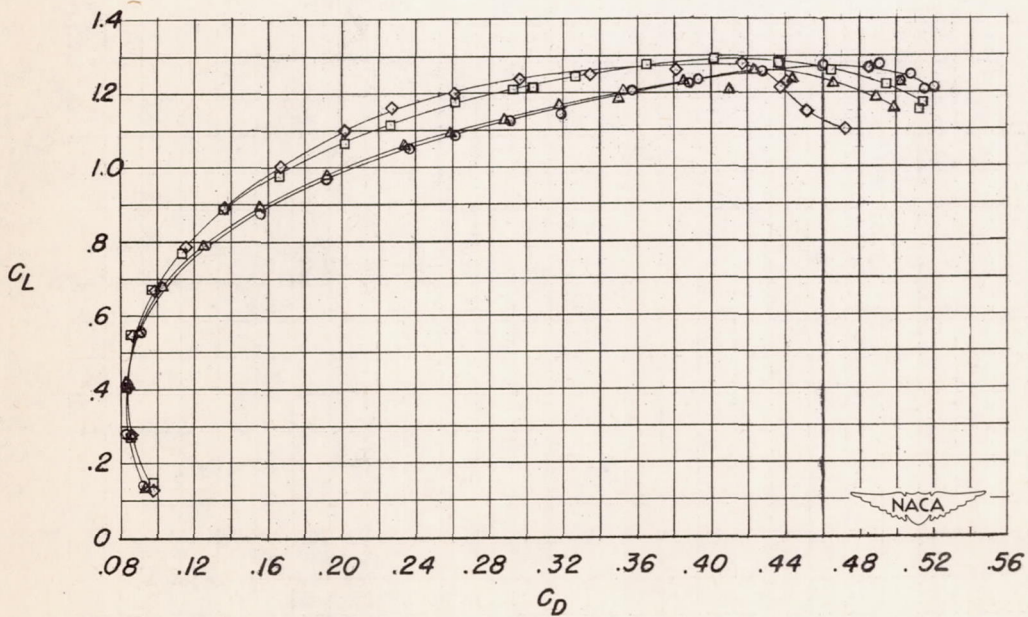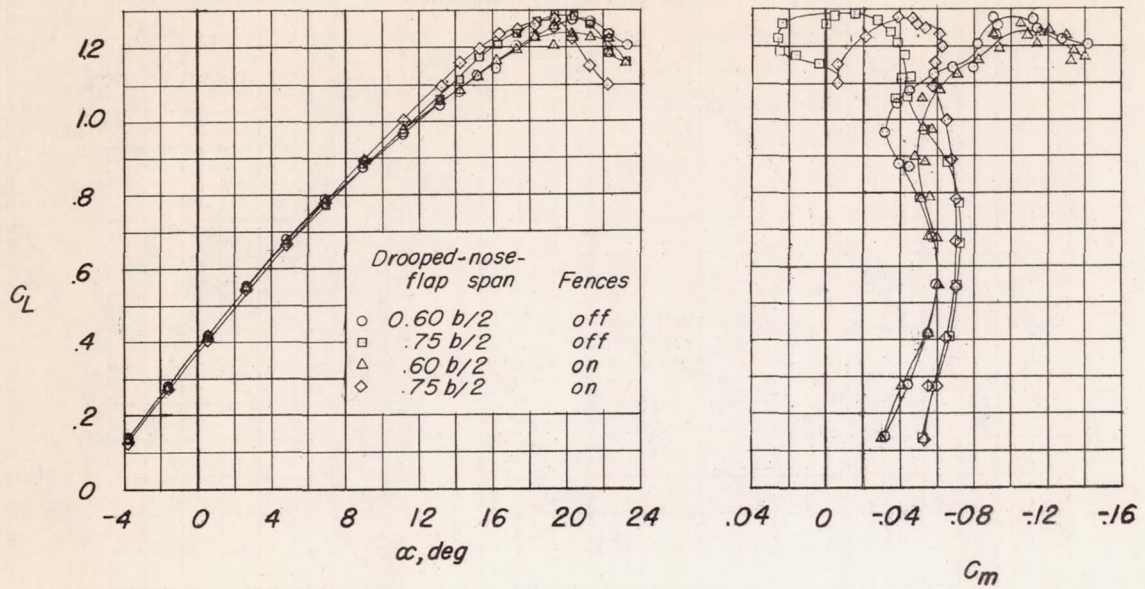
Figure 8.— Characteristics of a 42° sweptback wing with $0.60\frac{b}{2}$ and $0.75\frac{b}{2}$ drooped—nose flaps with and without upper—surface fences. $\delta_n = 30°$. Split flaps on.
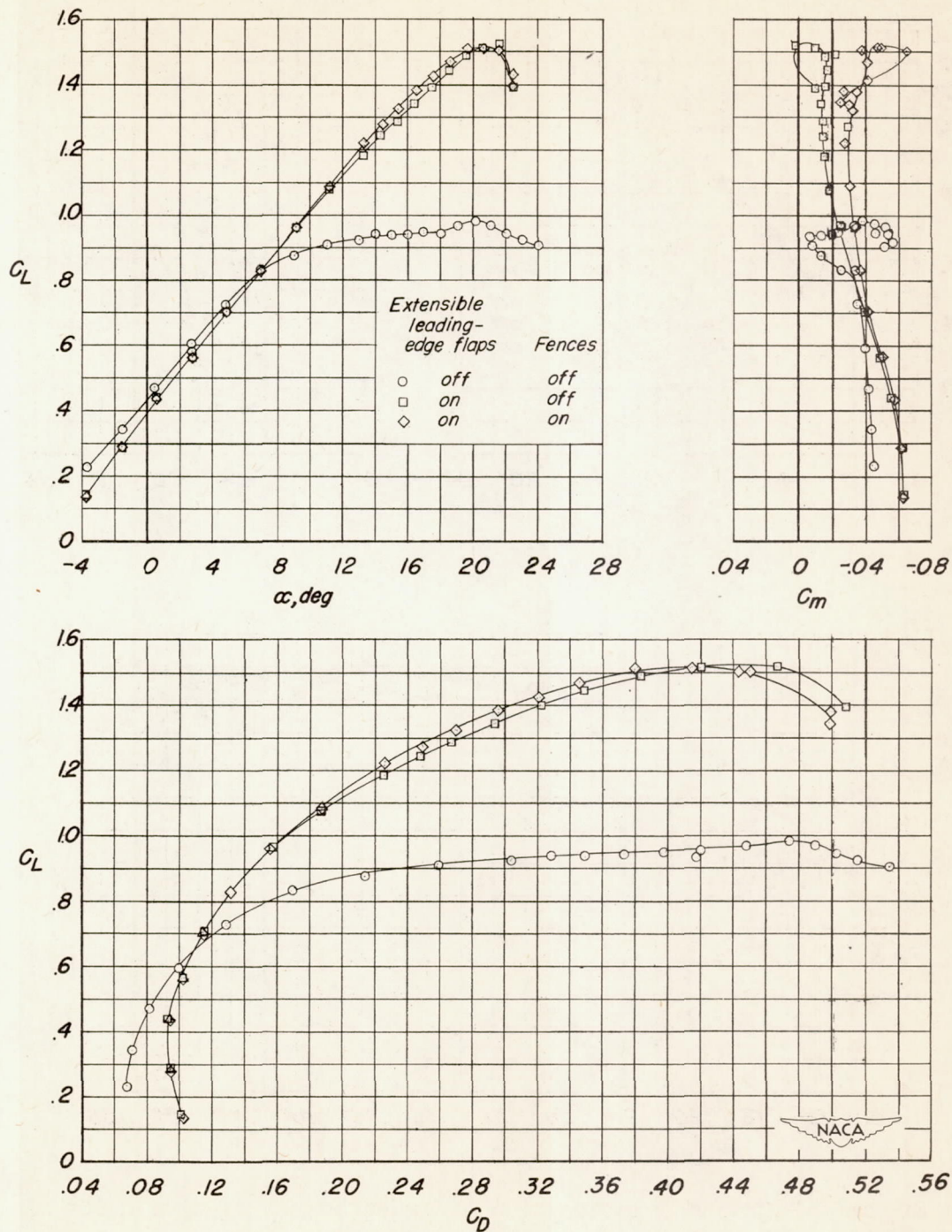
Figure 9.— Characteristics of a 42° sweptback wing with and without 0.70$\frac{b}{2}$ extensible leading—edge flaps and upper—surface fences. Split flaps on.
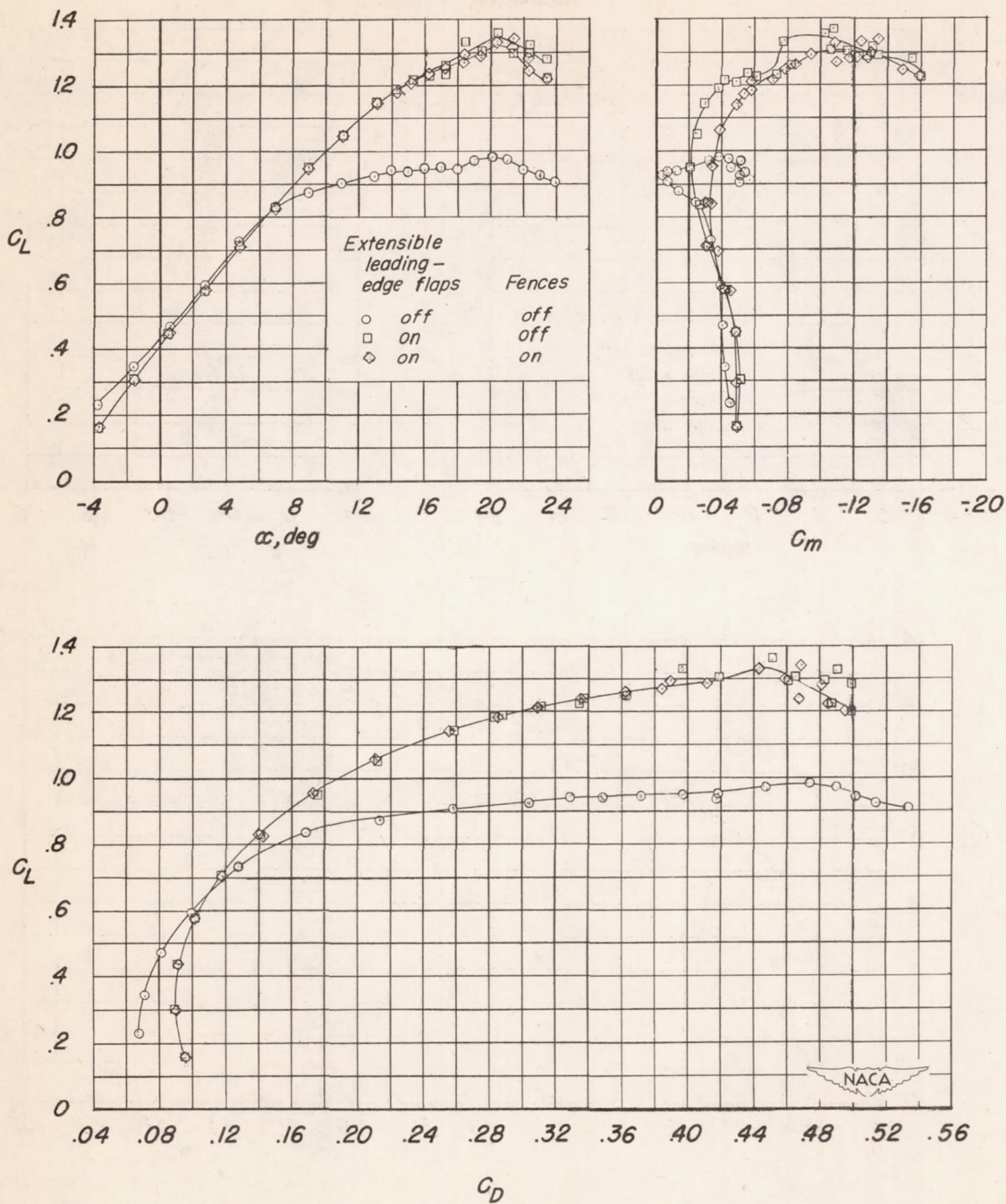
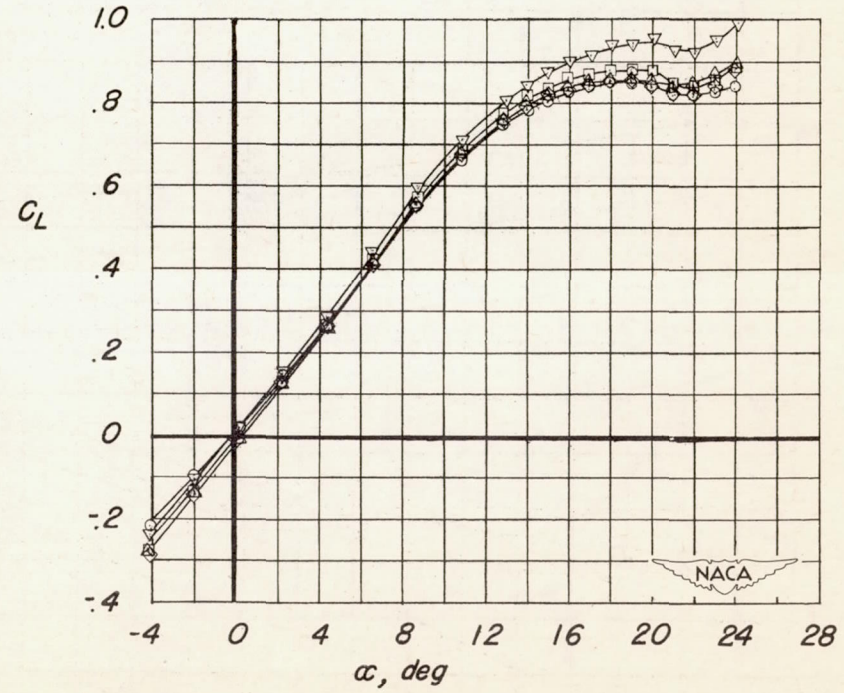Figure 10.— Characteristics of a 42° sweptback wing with and without
0.55$\frac{b}{2}$ extensible leading—edge flaps and upper—surface fences.
Split flaps on.
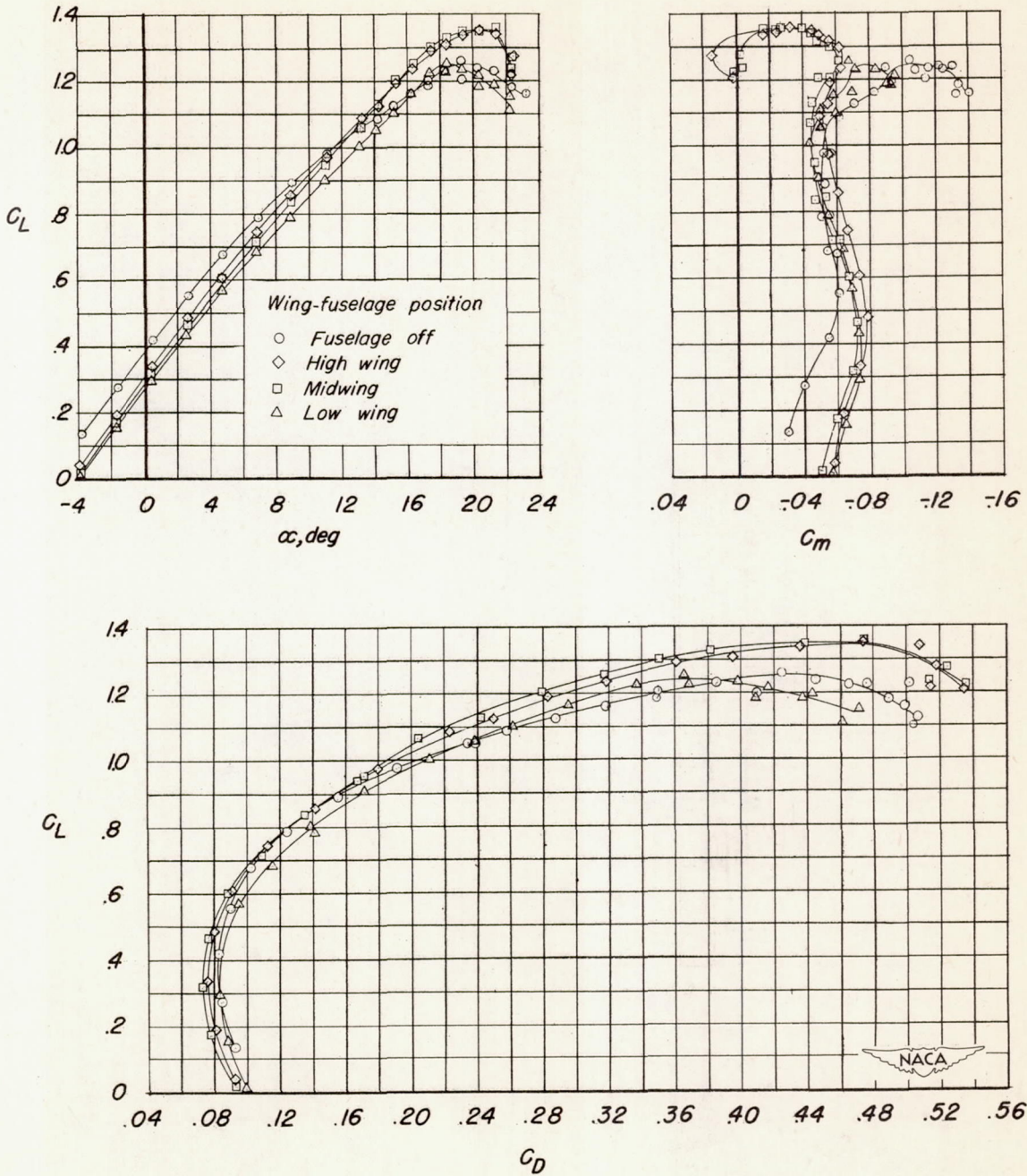
Figure 11.— Effects of wing—fuselage position on the characteristics of a 42° sweptback wing with $0.60\frac{b}{2}$ drooped—nose flaps, split flaps, and upper—surfaces fences. $\delta_n = 30°$.
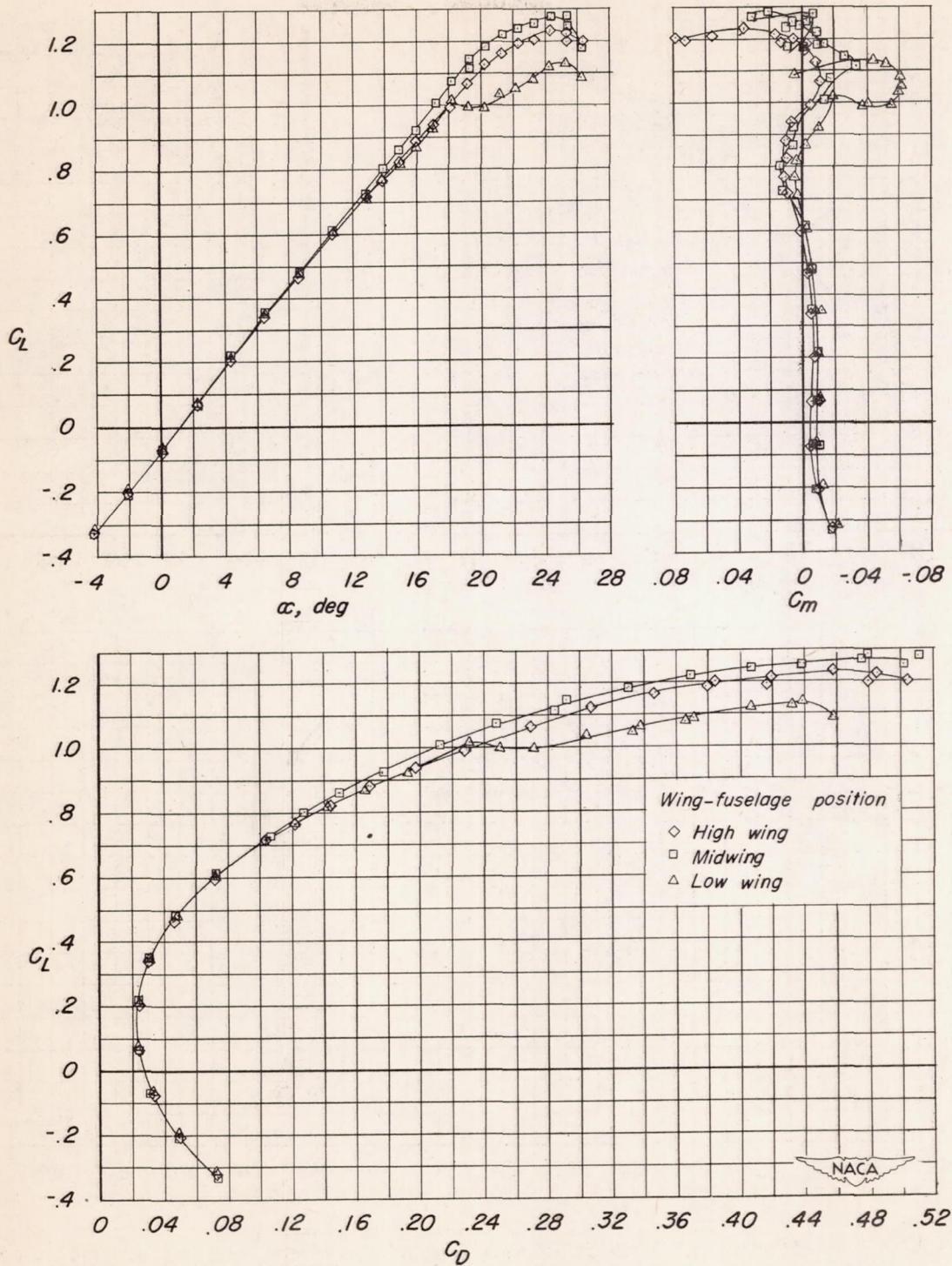
Figure 12.— Effects of wing—fuselage position on the characteristics of a
42° sweptback wing with $0.60\frac{b}{2}$ drooped—nose flaps and upper-surface
fences. $\delta_n = 30°$.
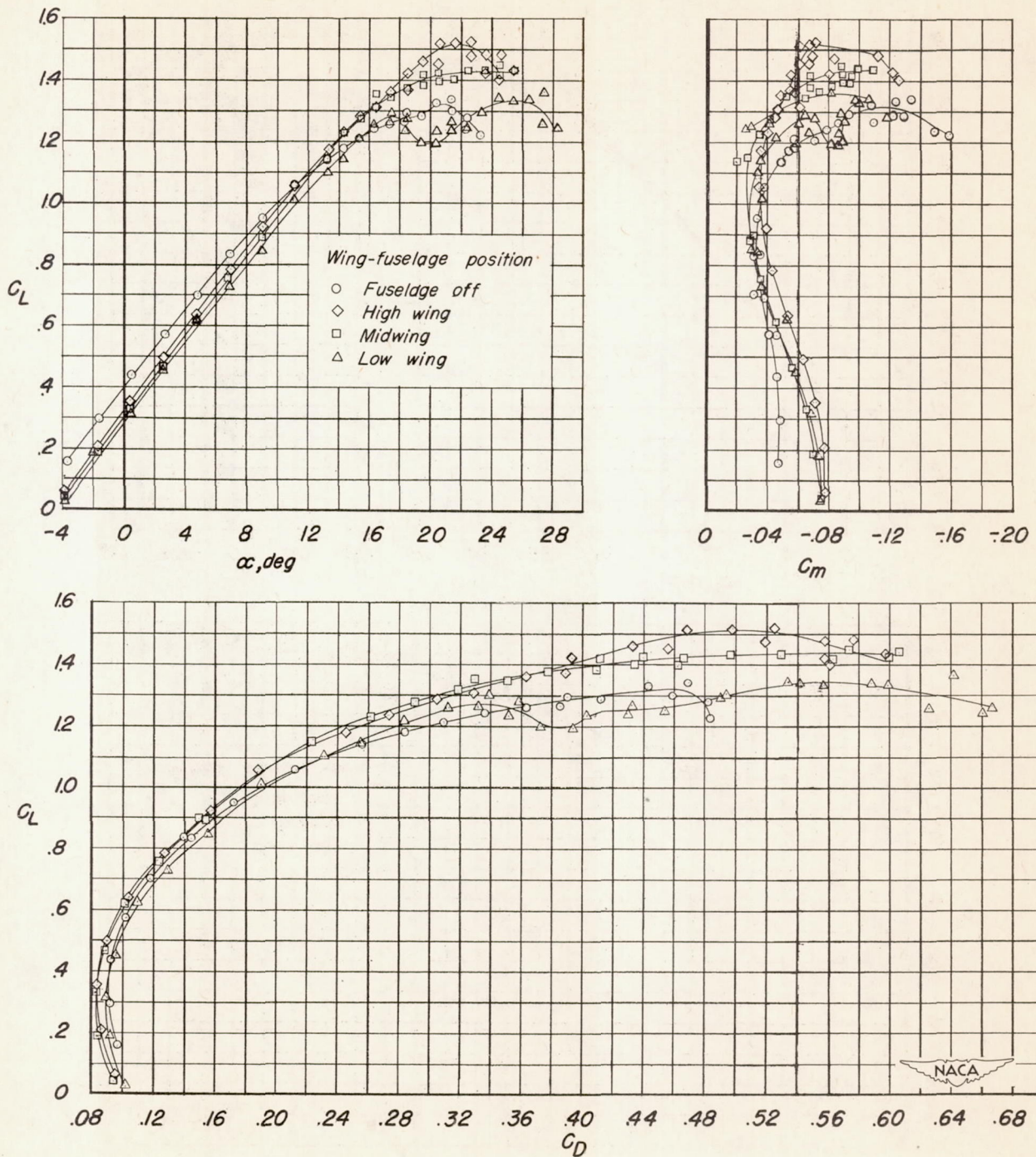
Figure 13.— Effects of wing-fuselage position on the characteristics of a 42° sweptback wing with $0.55\frac{b}{2}$ extensible leading-edge flaps, split flaps, and upper-surfaces fences.
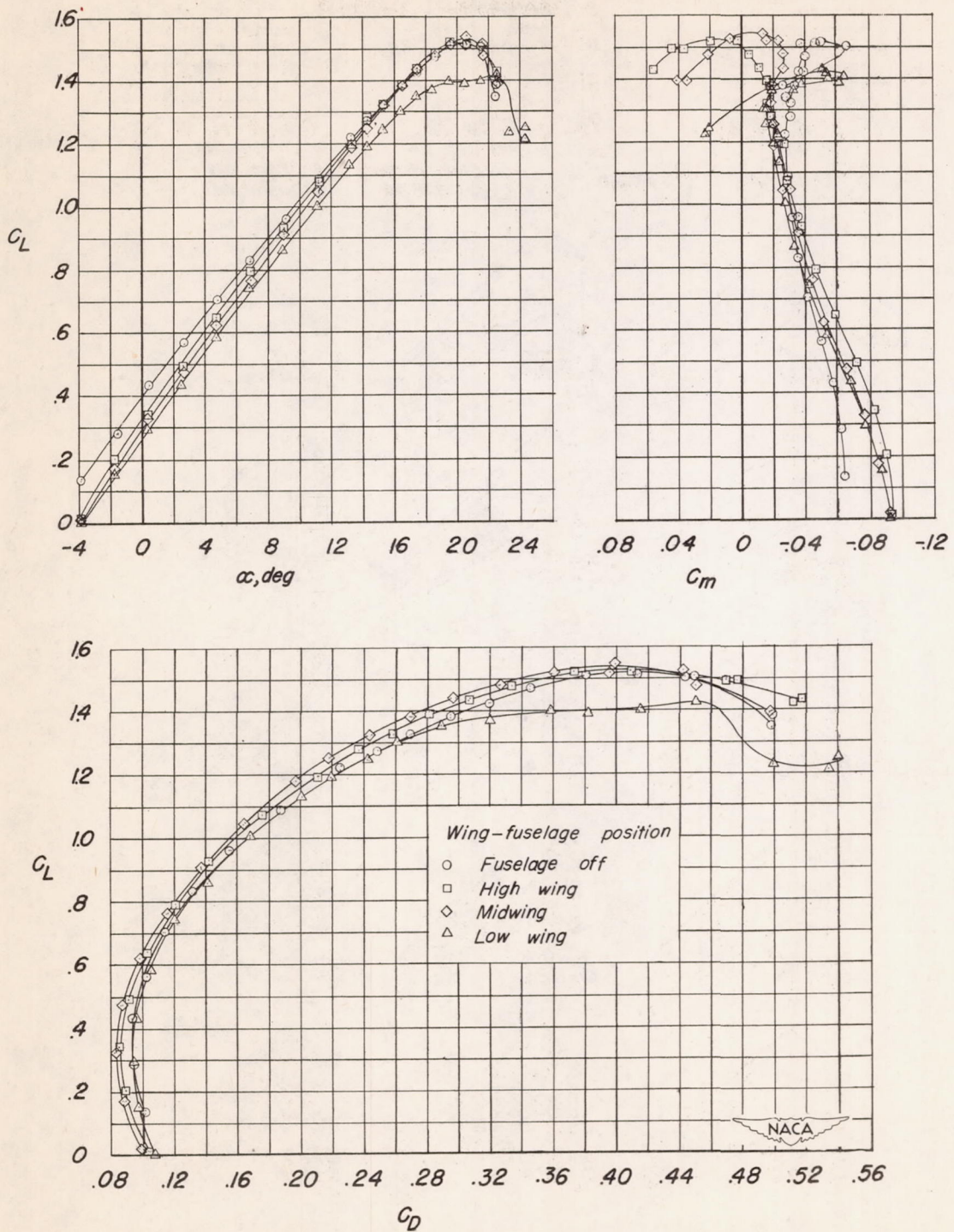
Figure 14.— Effects of wing—fuselage position on the characteristics of a
42° sweptback wing with $0.70\frac{b}{2}$ extensible leading—edge flaps, split flaps,
and upper—surface fences.
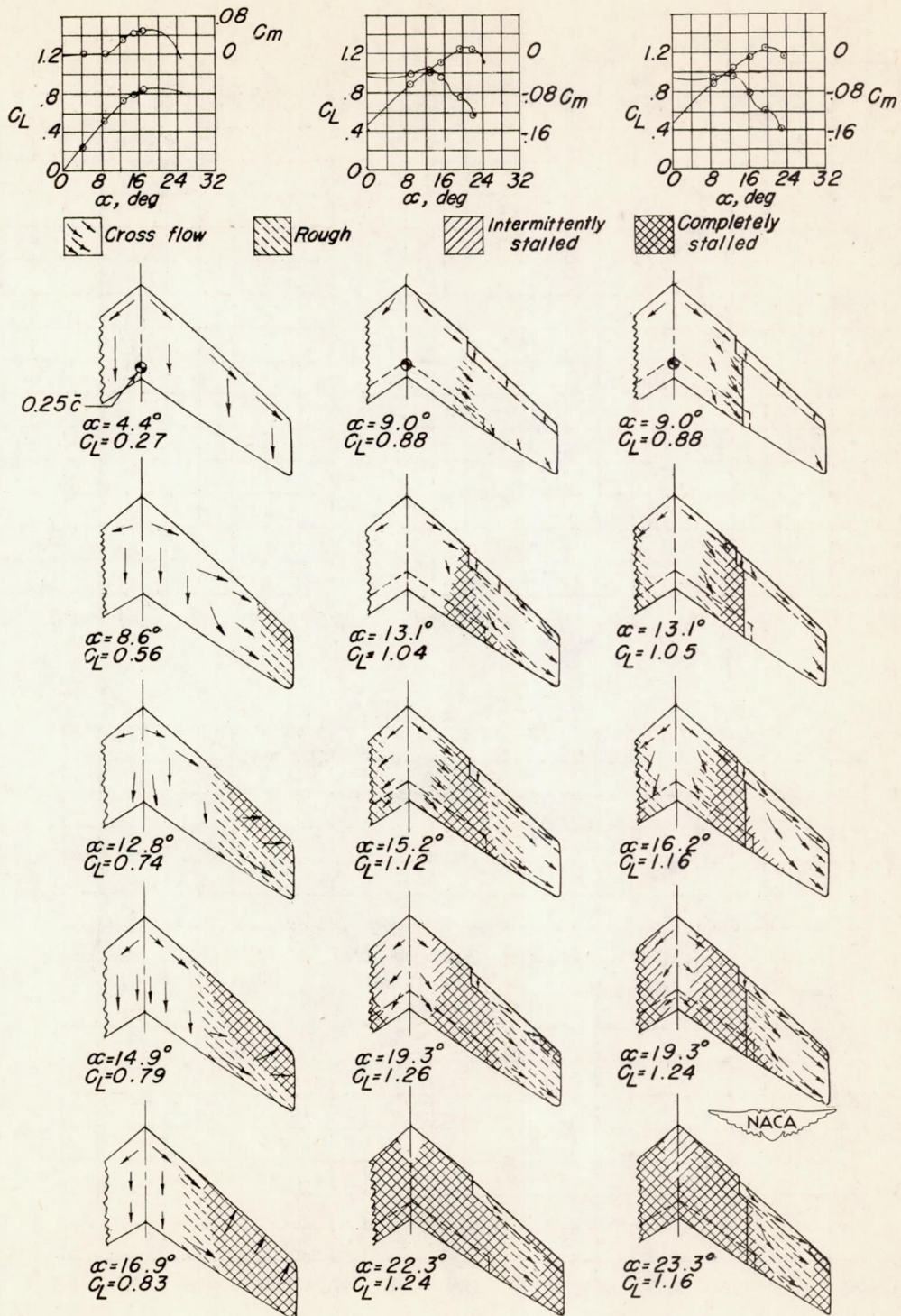
(a) Flaps off.   (b) $0.60\frac{b}{2}$ drooped

nose flaps deflected
$30°$. Split flaps on.

(c) $0.60\frac{b}{2}$ drooped nose
flaps deflected $30°$.
Split flaps and upper
surface fences on.

Figure 15.— Stalling characteristics of a $42°$ sweptback wing.
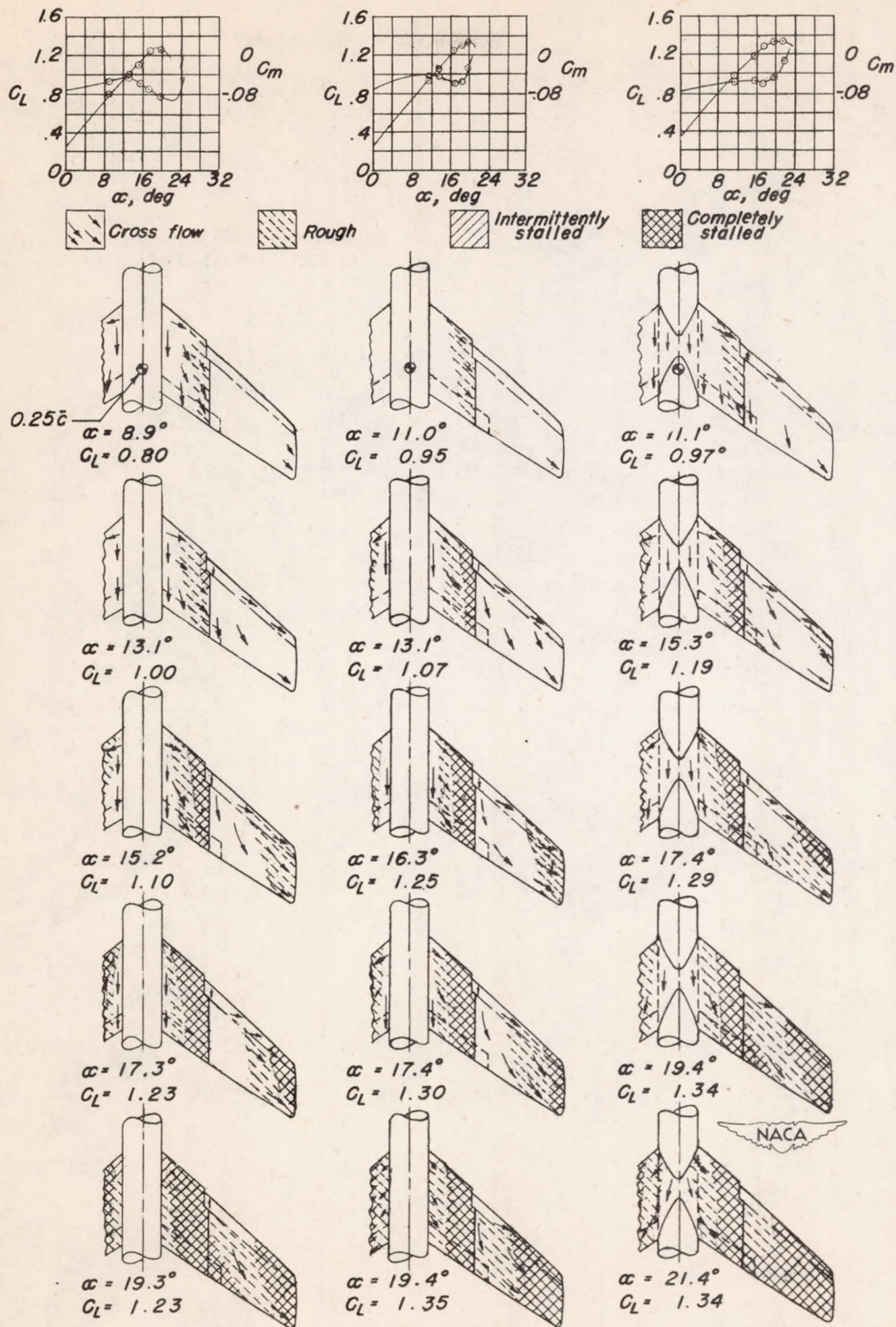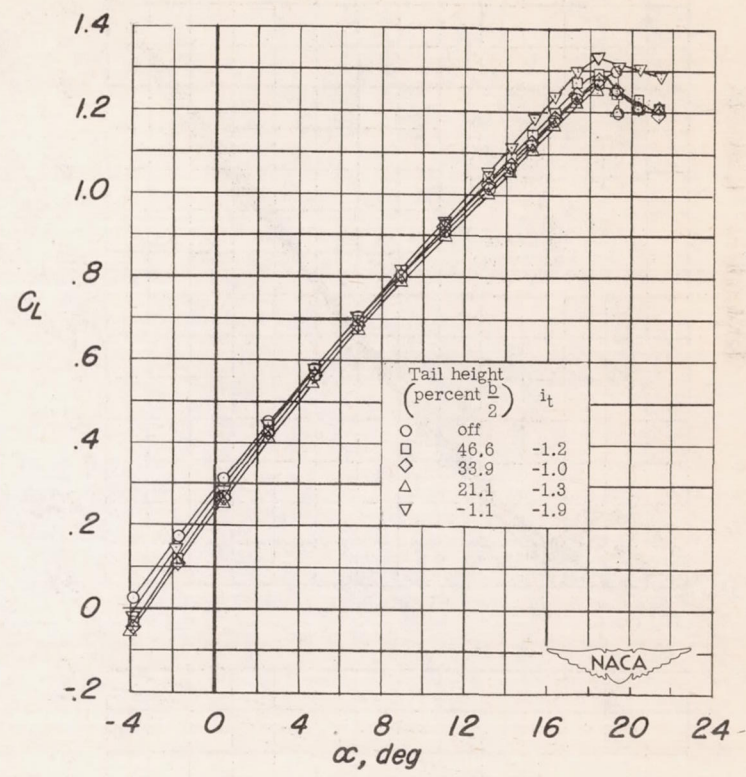
(a) Low wing.   (b) Midwing.   (c) High wing.

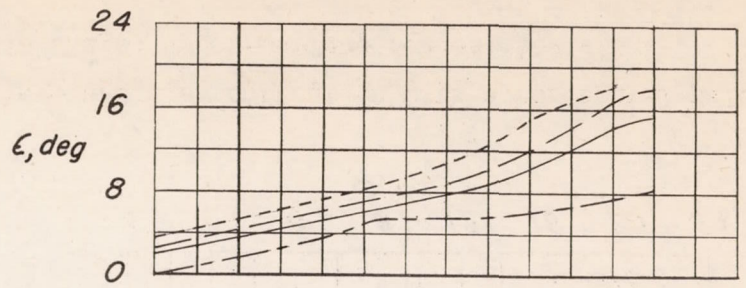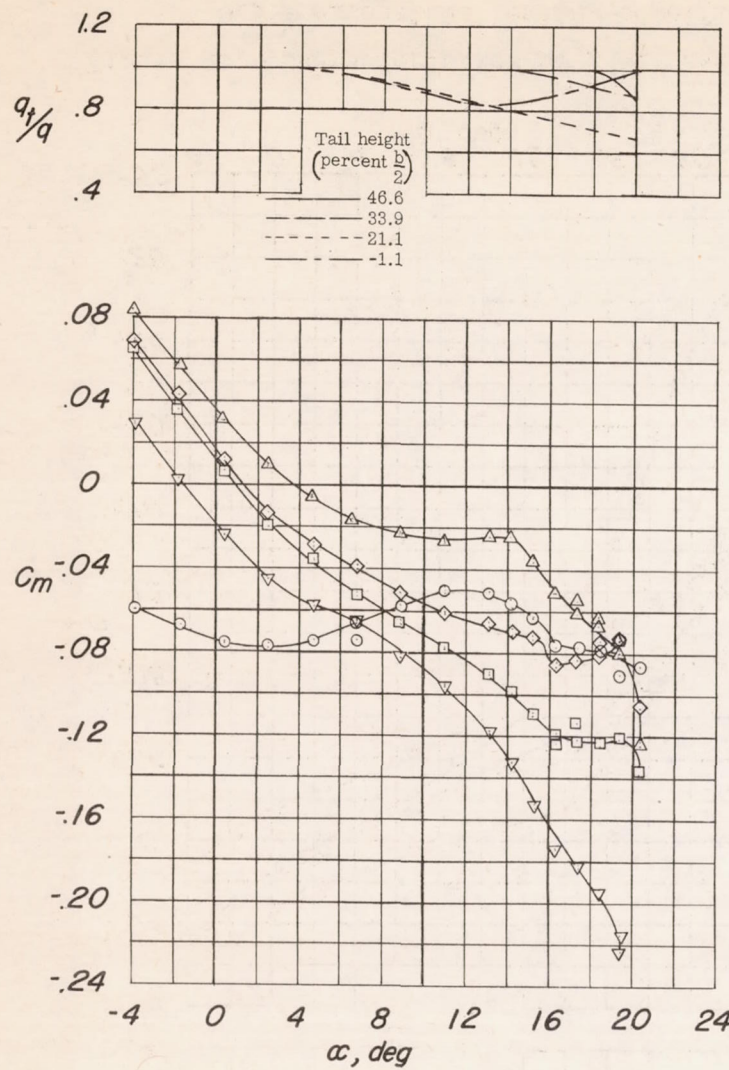Figure 16.— Stalling characteristics of a 42° sweptback wing—fuselage
combination with $0.60\frac{b}{2}$ drooped nose flaps, split flaps, and upper
surface fences.
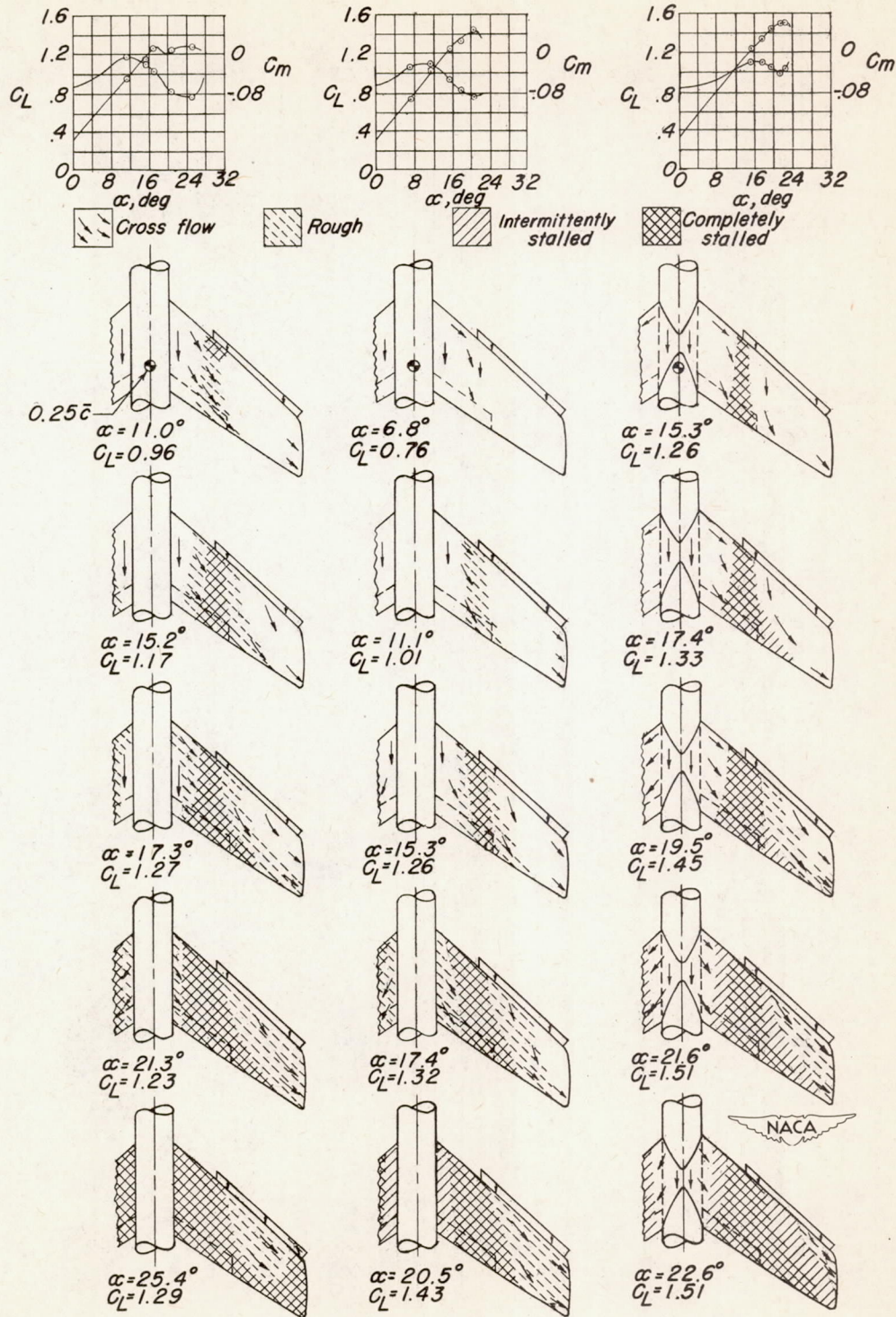
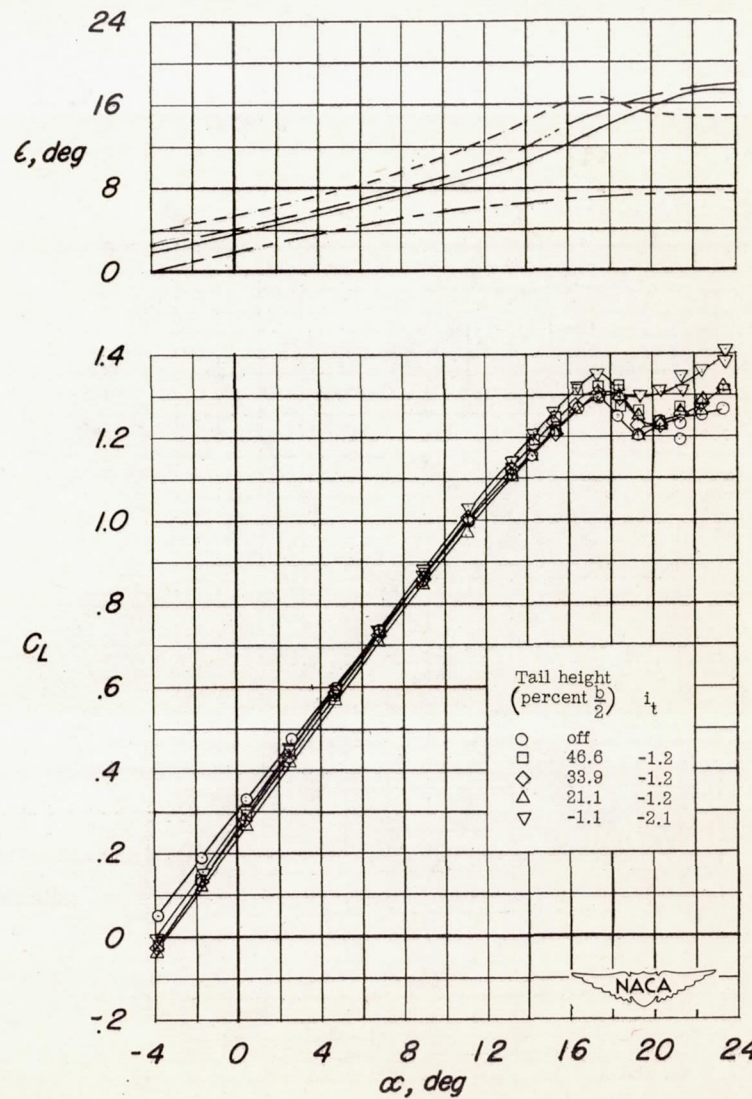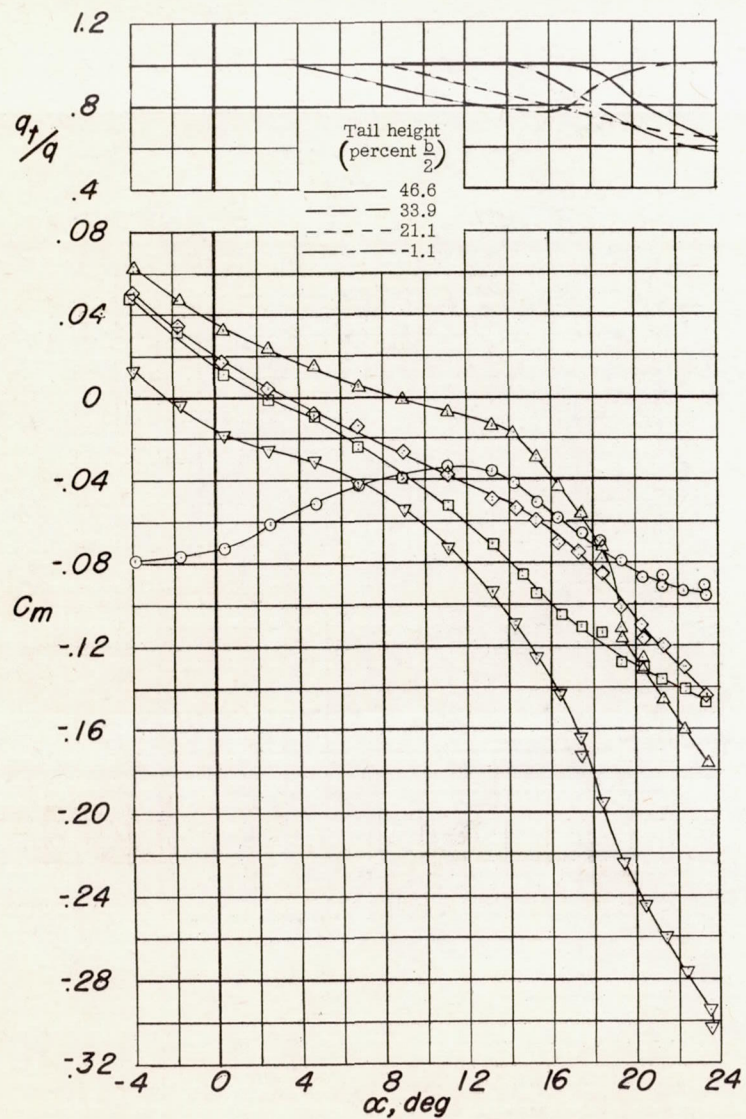(a) Low wing.   (b) Midwing.   (c) High wing.

Figure 17.— Stalling characteristics of a 42° sweptback wing—fuselage combination with $0.55\frac{b}{2}$ extensible leading-edge flaps and split flaps.

Gliding speed (mph)

Sinking speed (fps)

C_L

C_D

○ Flaps off

□ 0.60$\frac{b}{2}$ drooped-nose flaps; split flaps

△ 0.55$\frac{b}{2}$ extensible leading-edge flaps; split flaps

◇ 0.70$\frac{b}{2}$ extensible leading-edge flaps; split flaps

NACA
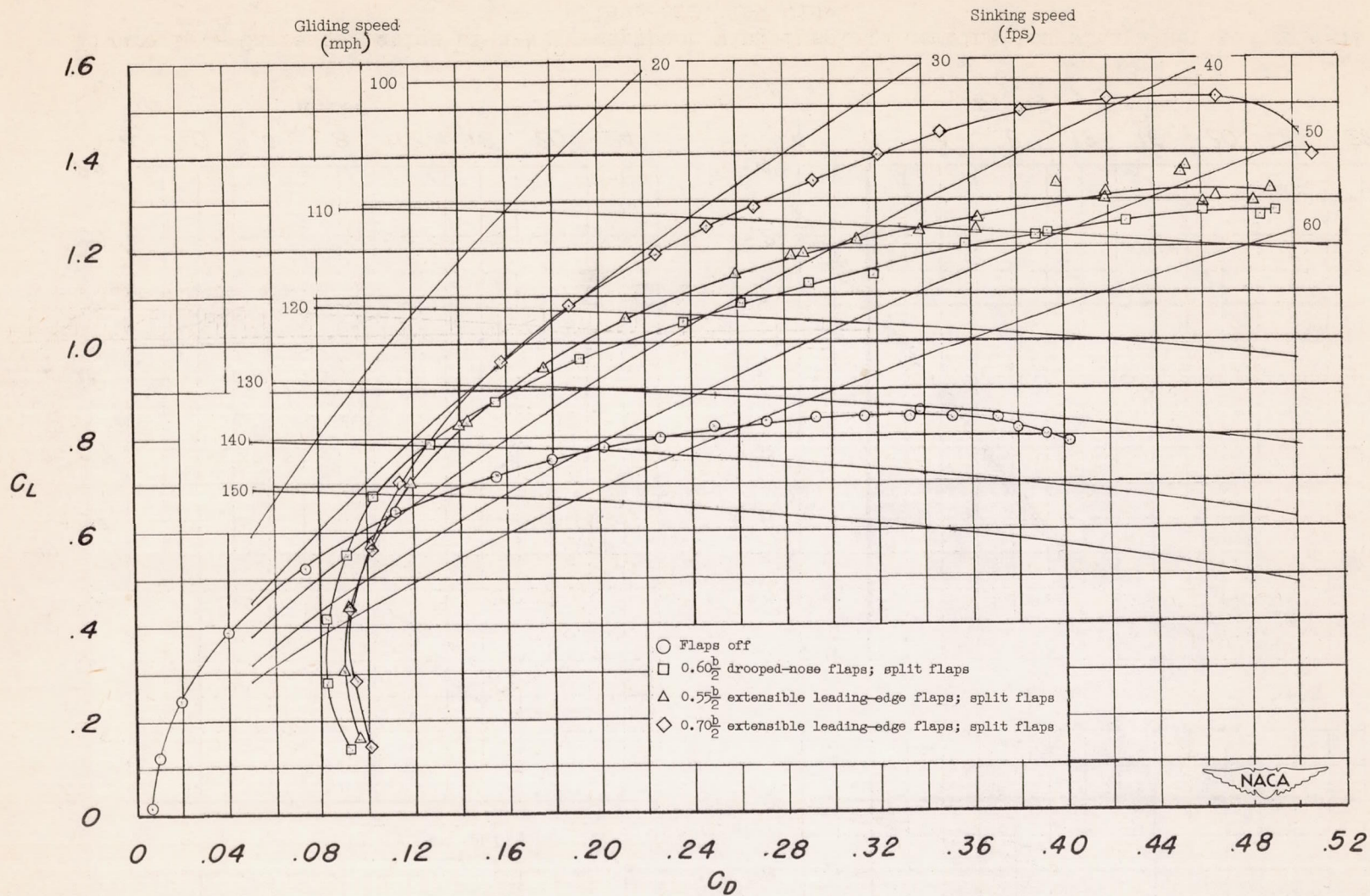
Figure 18.— Glide characteristics of a 42° sweptback wing for a wing loading of 40 pounds per square foot; standard sea-level conditions.
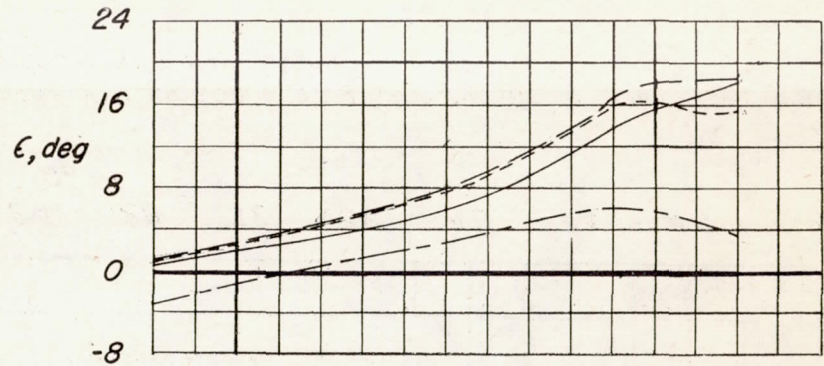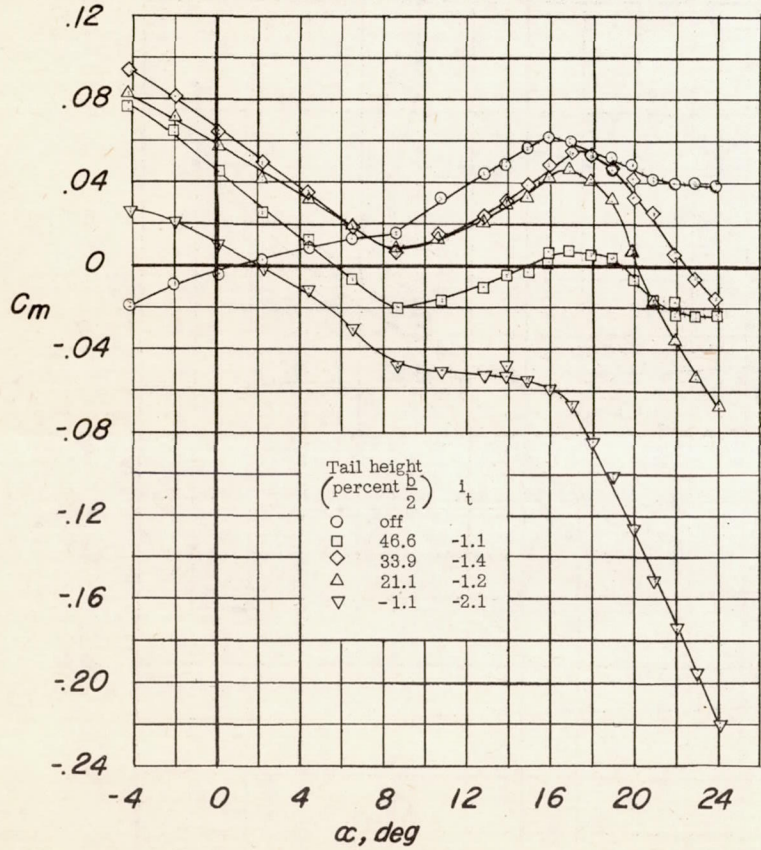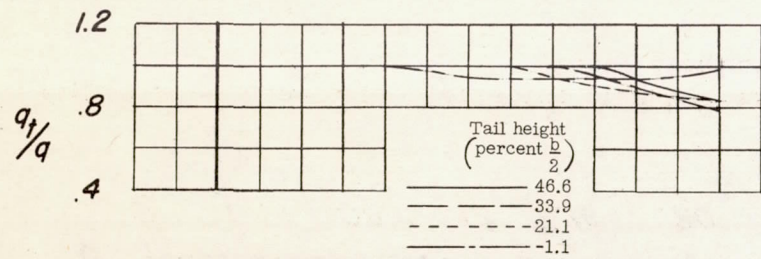
Figure 19.— Characteristics of a 42° sweptback wing–fuselage combination with a horizontal tail. Flaps off; low wing.

Figure 20.— Characteristics of a 42° sweptback wing—fuselage combination with horizontal tail. 0.60$\frac{b}{2}$ drooped—nose flaps; split flaps; upper—surface fences; low wing.

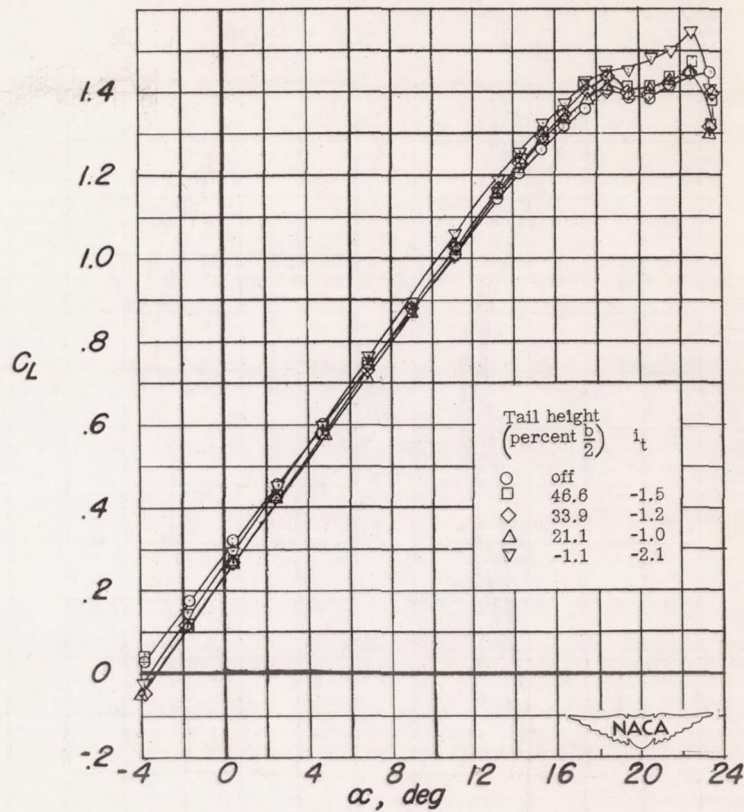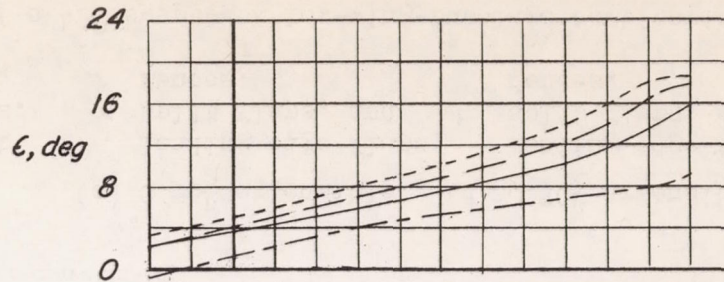Figure 21.— Characteristics of a 42° sweptback wing—fuselage combination with a horizontal tail. 0.55$\frac{b}{2}$ extensible leading—edge flaps; split flaps; upper—surface fences; low wing.
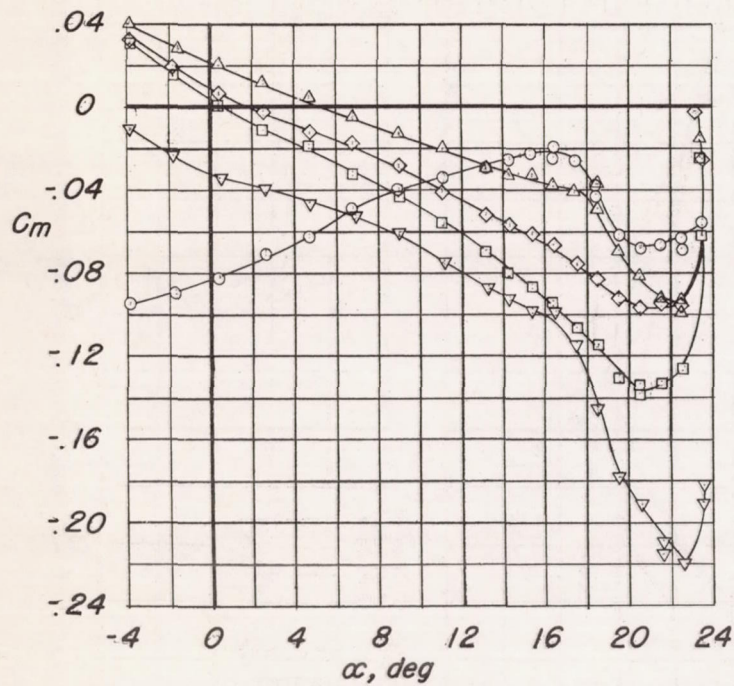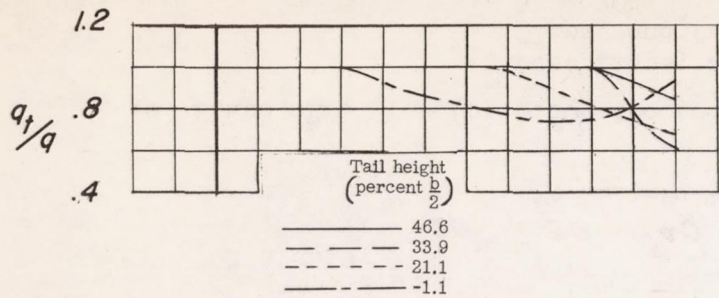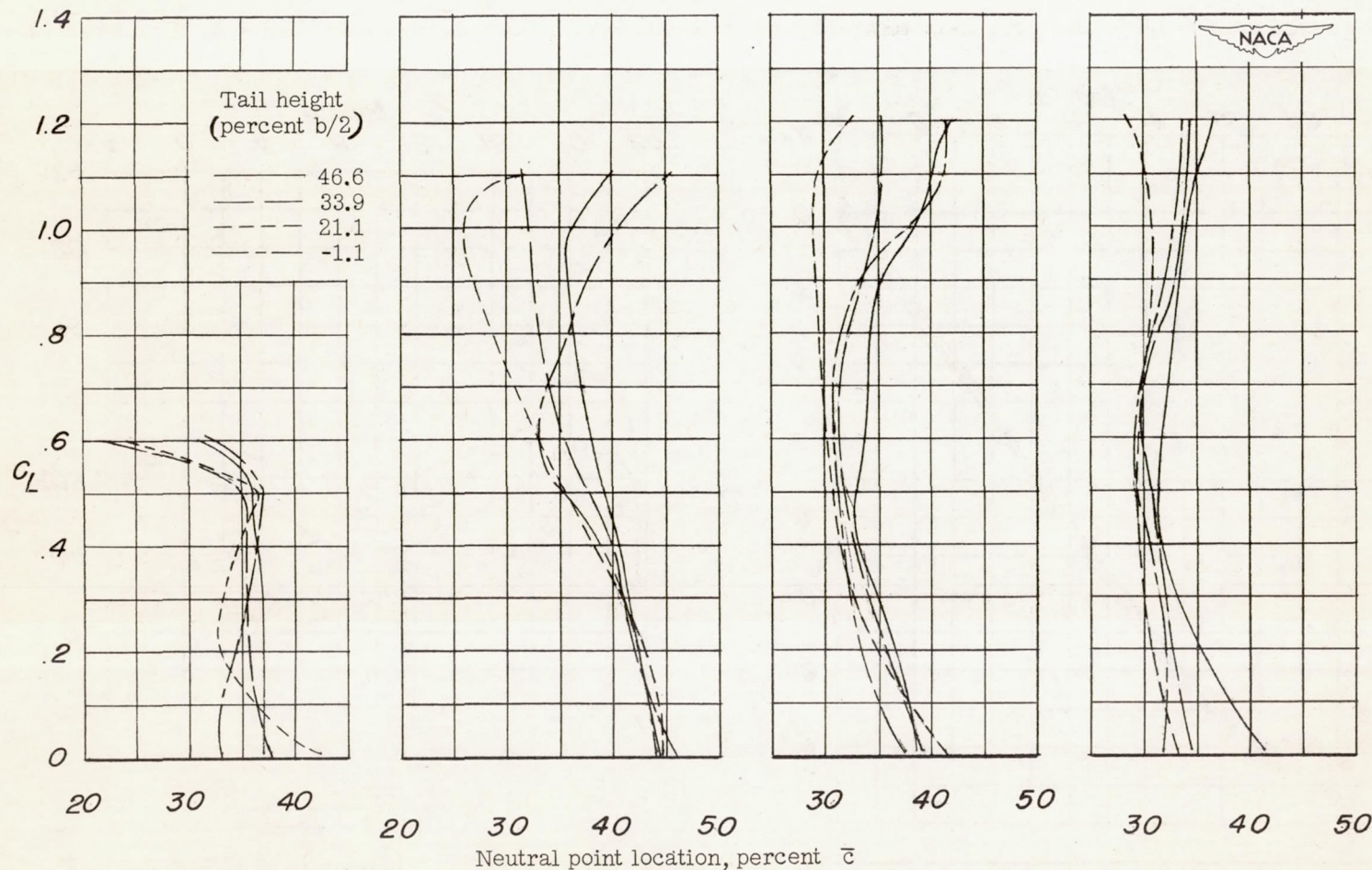
Figure 22.— Characteristics of a 42° sweptback wing—fuselage combination with a horizontal tail. 0.70$\frac{b}{2}$ extensible leading—edge flaps; split flaps; upper—surface fences; low wing.

Figure 23.— Neutral point characteristics of a 42° sweptback low–wing–fuselage combination.